NASA Contractor Report 178186

SIMPLE FORMULAS FOR STRAIN-ENERGY RELEASE RATES WITH HIGHER ORDER AND SINGULAR FINITE ELEMENTS

I. S. Raju

ANALYTICAL SERVICES & MATERIALS, INC.
Hampton, Virginia

Contracts NAS1-17808 and NAS1-18256
December 1986

National Aeronautics and Space Administration

Langley Research Center
Hampton, Virginia 23665

ABSTRACT

A general finite element procedure for obtaining strain-energy release rates for crack growth in isotropic materials is presented. The procedure is applicable to two-dimensional finite element analyses and uses the virtual crack-closure method. The procedure was applied to non-singular 4-noded (linear), 8-noded (parabolic), and 12-noded (cubic) elements and to quarter-point and cubic singularity elements. Simple formulas for strain-energy release rates were obtained with this procedure for both non-singular and singularity elements. The formulas were evaluated by applying them to two mode I and two mixed mode problems. Comparisons with results from the literature for these problems showed that the formulas give accurate strain-energy release rates.

INTRODUCTION

Two-dimensional finite element analyses are widely used to obtain stress-intensity factors and strain-energy release rates for cracked isotropic and orthotropic domains. Several methods are available to extract the stress-intensity factor K and hence the strain-energy release rate G from finite element results [1-5]. For isotropic materials, stress-intensity factors have been used to predict fatigue crack growth and fracture. However, for composites, idealized as orthotropic or anisotropic materials, with cracks or delaminations, the strain-energy

release rate G has been found to be more convenient [6,7] for these predictions.

The strain-energy release rate for a particular crack length can be obtained with two finite element analyses using the same model but with two crack lengths differing by a small amount. This procedure is not preferred since the boundary value problem needs to be solved twice. A variety of methods [8-10] which utilize only a single finite element analysis are available to obtain strain-energy release rates. One such method, based on Irwin's virtual crack-closure method, uses the stresses ahead of the crack tip and the displacements behind the crack tip. Rybicki and Kanninen [8] used this approach to obtain a simple formula for the strain-energy release rate for a cracked, isotropic domain modeled with four-noded quadrilateral, non-singular elements.

In the recent years, several crack-tip singularity elements have been developed [2,3,4,11,12]. These elements produce the required singularity at the crack tip and give accurate stress distributions with fewer degrees of freedom than non-singular elements. For the special singularity elements with the near-field solution built in explicitly [12], the K and G values are obtained as a part of the solution. For the more popular singularity elements, like the quarter-point (QP) and cubic singularity elements, K and G are usually obtained using the crack opening displacement (COD) method [2-5]. This procedure is attractive for isotropic materials but has not been applied for

cracks along interfaces in bimaterial plates and is difficult to apply for cracks in orthotropic or anisotropic plates.

The formula given by Rybicki and Kanninen [8] is attractive because the G values can be obtained easily from a single finite element analysis. Similar formulas would be very useful for higher order and singularity elements. The purpose of this paper is to present a uniform procedure for calculating strain-energy release rates that will apply to non-singular and singular elements of any order. The development of this procedure is based on Irwin's virtual crack-closure method. The procedure will provide a set of G formulas that depend on the crack opening displacements and the nodal forces at and ahead of the crack tip. The procedure outlined here will also serve as a basis for the development of similar formulas in the analysis of cracked orthotropic or anisotropic composite materials. These materials, however, are not considered in this paper.

First, Irwin's virtual crack-closure method is reviewed. Next, a general procedure for calculating strain-energy release rates that applies to linear and higher order elements is presented. The procedure is then extended to quarter-point and cubic singularity elements. Formulas for mixed-mode configurations are also obtained. Next, simpler versions of the formulas for the singularity elements are presented. The modifications required when the crack faces are loaded with a uniform pressure distribution are also presented. The G formulas are evaluated by comparing the calculated strain-energy release

rates with reference solutions from the literature for two mode I and two mixed-mode problems.

SYMBOLS

a	crack length
A_1, A_2, A_3, A_4	constants in assumed σ_y distribution
b	half-width of a center cracked tension specimen or width of a singe edge notch specimen
E	Young's modulus for a homogenous isotropic plate
E_1, E_2	Young's moduli in the bimaterial isotropic plate
F_{x_i}, F_{y_i}	nodal forces at the i^{th} node in the x- and y-directions, respectively
G, G_I, G_{II}	total, mode I, and mode II strain-energy release rates
h	half-height of specimen
K	stress-intensity factor
$[Q]$	transformation matrix connecting forces F_{x_i} or F_{y_i} and constants A_i
r	distance behind the crack tip on the y=0 line
S	uniform remote stress or uniform crack-face pressure loading
u, v	displacements in the x- and y-directions, respectively
$\tilde{u}_m$, $\tilde{v}_m$	relative displacements u and v of node m with respect to the crack tip node i: $\tilde{u}_m = u_m - u_i$; $\tilde{v}_m = v_m - v_i$

$v(x)$	displacement interpolation function of a finite element
$v_R(r)$	relative crack opening displacement at a distance r behind the crack tip
x, y	Cartesian coordinates
σ_x, σ_y, σ_{xy}	Cartesian stresses
ν, ν_1, ν_2	Poisson's ratios for isotropic, homogeneous and bimaterial plates
Δ	crack growth increment, equal to the length of the element nearest to the crack tip in the x-direction

VIRTUAL CRACK-CLOSURE METHOD

Figure 1(a) shows a crack tip in an infinite isotropic plate subjected to remote mode I type loading. The normal stress distribution ahead of the crack tip and on the $y = 0$ line is of the form

$$\sigma_y = \frac{A_1}{\sqrt{x}} + A_2 + A_3\sqrt{x} + \ldots \qquad (1)$$

If the crack extends from a to $a + \Delta$, for infinitismal values of Δ, the crack opening displacements behind the new crack tip will be approximately the same as those behind the original crack tip. Then the work necessary to extend the crack from a to $a + \Delta$ is the same as that necessary to close the crack tip from $a + \Delta$ to a. Irwin computed this work as

$$W = \frac{1}{2} \int_0^{\Delta} v(r)\, \sigma_y(\Delta - r)\, dr \qquad (2)$$

where $v(r)$ is the crack opening displacement at a distance r

behind the crack tip at $a + \Delta$. He then obtained the strain-energy release rate as

$$G = \lim_{\Delta \to 0} \frac{W}{\Delta} = \lim_{\Delta \to 0} \frac{1}{2\Delta} \int_0^{\Delta} v(r)\sigma_y(\Delta - r)\, dr \qquad (3)$$

Rybicki and Kanninen [8] used Eq. (3) in their finite element analysis. They considered models with 4-noded quadrilateral elements only. The strain-energy release rate equations from Ref. [8] are

$$G_I = \frac{1}{2\Delta} \{F_{y_i}(v_k - v_{k'})\} \qquad (4)$$

$$G_{II} = \frac{1}{2\Delta} \{F_{x_i}(u_k - u_{k'})\}$$

where F_{x_i} and F_{y_i} are the nodal forces at node i in the x- and y-directions, respectively, computed from elements I and J in Fig. 1(b). The terms u_k and v_k are the displacements at node k in the x- and y-directions, respectively. The formulas in Eqs. (4) are very attractive because the G values can be computed from a single finite element analysis. These equations were shown to give accurate G values.

Simple formulas, like Eqs. (4), will be very useful for higher order or singularity elements. This paper develops a uniform procedure, based on Irwin's virtual crack-closure method, that will give simple formulas for the strain-energy release rates for higher order and singularity elements.

PROCEDURE FOR CALCULATING STRAIN-ENERGY RELEASE RATES

In this section, a general procedure for obtaining the strain-energy release rates from a single finite element analysis is presented. First, this procedure is outlined for 4-noded quadrilateral elements. The procedure is then extended to 8-noded parabolic and 12-noded cubic elements. This procedure is also used to obtain G formulas for quarter-point (QP) and cubic singularity elements.

In this procedure, the following assumptions are made:

1. The finite element idealization in the immediate vicinity of the crack tip is symmetric about the x = 0 line and symmetric about the crack plane (y = 0).
2. The normal and shear stresses on the y = 0 line and ahead of the crack tip are assumed to have the classical square-root stress distribution as in Eq. (1). In the limit, as the element size in the analysis domain becomes smaller, the classical square-root distribution will develop near the crack tip. This is true regardless of the type of element used to model the problem. Therefore, the form of Eq. (1) is assumed a priori instead of using the stress distribution given by the particular finite element model.
3. The functional form of the crack opening profiles, u(r) and v(r), on the y = 0 line is determined by the element shape functions.

The normal stress σ_y distribution of Eq. (1) can be determined from the nodal forces at and ahead of the crack tip (on the y = 0 line). While nodal forces are available at several nodes on the y = 0 line, in this procedure only the nodal forces from elements nearest to and around the crack tip will be used to determine the σ_y distribution. Then the normal stress σ_y and the crack opening displacements v(r) are used in Irwin's virtual crack-closure method to obtain the G formulas for various higher order non-singular and singularity elements.

Non-Singular Elements

4-Noded Quadrilateral Elements

Consider a finite element idealization with linear quadrilateral elements symmetric about the crack tip as shown in Fig. 2. Ahead of the crack tip (at node i) and along the y = 0 line, the stress σ_y is assumed to have the form

$$\sigma_y = \frac{A_1}{\sqrt{x}} + A_2 \quad \text{for } x \geq 0 \tag{5a}$$

$$= 0 \quad \text{for } x < 0 \tag{5b}$$

where A_1 and A_2 are unknown constants. The nodal forces F_{y_i}, F_{y_j}, F_{y_l}, F_{y_m} shown in Fig. 2(b) can be thought of as consistent nodal forces acting at nodes i, j, l, m due to a prescribed stress distribution of the form in Eq. (5). Conversely, using these nodal forces, one could calculate the

constants in the assumed stress distribution of Eq. (5) ahead of the crack tip along the x-axis.

The stress distribution in Eq. (5a) is valid only in the immediate vicinity of the crack tip since it is obtained from the near field solution at the crack tip. Also, since there are two unknown constants in the assumed distribution of Eq. (5a), two forces are sufficient to determine the constants. The two forces F_{y_i} and F_{y_j}, computed from elements I and J nearest to and around the crack tip, can be used. These elements are shown by solid lines in Fig 2(b).

The work done by the assumed stress distribution on the boundary displacements of elements I and J is equated to the work performed by the forces F_{y_i} and F_{y_j} on the displacements v_i and v_j as

$$\frac{1}{2} \int_0^{\Delta} \sigma_y(x)\, v(x)\, dx = -\frac{1}{2} \left[F_{y_i} v_i + F_{y_j} v_j\right] \qquad (6)$$

where $v(x)$ is the displacement interpolation function of the 4-noded element and Δ is the element length. Since a tensile σ_y stress causes forces in the negative y-direction, a negative sign appears in Eq. (6). For this linear quadrilateral element, the $v(x)$ on the ij side is

$$v(x) = \left[1 - \frac{x}{\Delta}\right] v_i + \left(\frac{x}{\Delta}\right) v_j \qquad (7)$$

Substituting Eq. (7) into Eq. (6) and equating the multipliers of v_i and v_j yields

$$F_{y_i} = -\int_0^{\Delta} \left[\frac{A_1}{\sqrt{x}} + A_2\right]\left(1 - \frac{x}{\Delta}\right)dx = -\left(\frac{4}{3}\sqrt{\Delta}\,A_1 + \left(\frac{\Delta}{2}\right)A_2\right)$$

$$F_{y_j} = -\int_0^{\Delta} \left[\frac{A_1}{\sqrt{x}} + A_2\right]\left(\frac{x}{\Delta}\right)dx = -\left(\frac{2}{3}\sqrt{\Delta}\,A_1 + \left(\frac{\Delta}{2}\right)A_2\right) \qquad (8)$$

Eq. (8) may be written as

$$\{F\} = [Q]\{A\} \qquad (9)$$

where

$$\{F\} = \{F_{y_i} \quad F_{y_j}\}^T$$

$$\{A\} = \{A_1\sqrt{\Delta} \quad A_2\Delta\}^T$$

and

$$[Q] = -\frac{1}{6}\begin{bmatrix} 8 & 3 \\ 4 & 3 \end{bmatrix}$$

Substitution of the calculated values of A_1 and A_2 from Eq. (9) in Eq. (5) expresses the stress distribution σ_y ahead of the crack tip completely in terms of nodal forces F_{y_i} and F_{y_j}.

Now consider the displacements behind the crack tip. The relative crack opening displacement v_R at any distance r from the crack tip can be determined by the nodal displacements of nodes i, k and k' and the element shape functions as

$$v_R(r) = \left(1 - \frac{r}{\Delta}\right) v_i + \frac{r}{\Delta}\left(v_k - v_{k'}\right) \qquad (10)$$

Now that the stress distribution ahead of the crack tip and the relative displacements behind the crack tip are known,

Irwin's approach can be used to calculate the strain-energy release rates as

$$G_I = \lim_{\Delta \to 0} \frac{1}{2\Delta} \int_0^{\Delta} \sigma_y(\Delta - r)\, v_R(r)\, dr \tag{11a}$$

$$= \lim_{\Delta \to 0} \frac{1}{2\Delta} \int_0^{\Delta} \left[\frac{A_1}{\sqrt{\Delta - r}} + A_2\right] \left[\left(1 - \frac{r}{\Delta}\right) v_i + \frac{r}{\Delta} (v_k - v_{k'}) \right] dr \tag{11b}$$

Integrating Eq. (11b) and using Eq. (9) gives

$$G_I = \lim_{\Delta \to 0} - \frac{1}{2\Delta} \left[F_{y_j} v_i + F_{y_i} (v_k - v_{k'})\right] \tag{12}$$

Because the relative displacement at the crack tip v_i is zero, Eq. (12) reduces to

$$G_I = \lim_{\Delta \to 0} \left(- \frac{1}{2\Delta} \left[F_{y_i} (v_k - v_{k'})\right]\right) \tag{13}$$

A similar procedure can be followed to show that

$$G_{II} = \lim_{\Delta \to 0} \left(- \frac{1}{2\Delta} \left[F_{x_i} (u_k - u_{k'})\right]\right) \tag{14}$$

The limits in Eqs. (13) and (14) suggest that the crack tip element needs to be small, and as smaller elements are used at the crack tip, the correct limits for G_I and G_{II} are approached. Numerical experimentation is required to determine the necesary mesh refinement and the limits in Eqs. (13) and (14) can be then dropped in actual computations.

Eqs. (13) and (14) are identical to those presented by Rybicki and Kanninen [8] and are widely used in the literature [13-15]. Equations (13) and (14) are also applicable if triangular elements (Fig. 2(c)), obtained by collapsing the quadrilateral elements, are used at the crack tip. Note that for this idealization, the forces F_{y_i} and F_{y_j} are the forces at nodes i and j computed from elements I, J, K and L surrounding the crack tip.

8-Noded Parabolic Element

To obtain the G expressions for the 8-noded element, the procedure outlined above is followed. For this element, because forces are available at three nodes, i, j, and k (see Fig. 3(a)), the σ_y distribution along the y = 0 line is assumed to be

$$\sigma_y = \frac{A_1}{\sqrt{x}} + A_2 + A_3\sqrt{x} \tag{15}$$

The parabolic shape functions for this element are

$$v(x) = \left(1 - \frac{3x}{\Delta} + \frac{2x^2}{\Delta^2}\right) v_i + \left(4\frac{x}{\Delta} - 4\frac{x^2}{\Delta^2}\right) v_j + \left(-\frac{x}{\Delta} + 2\frac{x^2}{\Delta^2}\right) v_k \tag{16}$$

As before, the forces at the nodes i, j, and k can be related to the constants A_1, A_2, and A_3 of the assumed σ_y

distribution (Eq. (15)) as

$$\{F\} = [Q]\{A\} \tag{17}$$

where

$$\{F\} = \{F_{y_i} \quad F_{y_j} \quad F_{y_k}\}^T$$

$$\{A\} = \{A_1\sqrt{\Delta} \quad A_2\Delta \quad A_3\Delta^{3/2}\}^T$$

and

$$[Q] = -\frac{1}{210}\begin{bmatrix} 168 & 35 & 8 \\ 224 & 140 & 96 \\ 28 & 35 & 36 \end{bmatrix}$$

The strain-energy release rates are obtained by performing the integrations as in Eq. (11a) and using Eq. (17) as

$$G_I = -\frac{1}{2\Delta}\left[F_{y_i}(v_m - v_{m'}) + F_{y_j}(v_l - v_{l'})\right]$$

$$G_{II} = -\frac{1}{2\Delta}\left[F_{x_i}(u_m - u_{m'}) + F_{x_j}(u_l - u_{l'})\right] \tag{18}$$

Note that the forces at node k do not appear in these equations because the relative displacement at node i is zero.

These equations are similar to those for the 4-noded element. Eqs. (18) are also applicable if triangular parabolic elements (Fig. 3(b)), obtained by collapsing the parabolic elements, are used at the crack tip. Equations (18) were used in references 6, 7 and 16 to obtain G values for delaminated

composite laminates. Recently, Krishnamurthy et. al [17], using a procedure similar to the one described in this paper, derived G formulas identical to Eqs. (18) for this element.

12-Noded Cubic Element

For this element, because four forces are available at nodes i, j, k, and l (see Fig. 3(c)), the σ_y distribution along the y = 0 line is assumed to be

$$\sigma_y = \frac{A_1}{\sqrt{x}} + A_2 + A_3\sqrt{x} + A_4 x \tag{19}$$

The cubic shape functions for this element are

$$\begin{aligned} v(x) = {} & [1 - \frac{11}{2}\frac{x}{\Delta} + 9(\frac{x}{\Delta})^2 - (\frac{9}{2})(\frac{x}{\Delta})^3]v_i \\ & + [9(\frac{x}{\Delta}) - (\frac{45}{2})(\frac{x}{\Delta})^2 + (\frac{27}{2})(\frac{x}{\Delta})^3]v_j \\ & + [-(\frac{9}{2})(\frac{x}{\Delta}) + 18(\frac{x}{\Delta})^2 - (\frac{27}{2})(\frac{x}{\Delta})^3]v_k \\ & + [(\frac{x}{\Delta}) - (\frac{9}{2})(\frac{x}{\Delta})^2 + (\frac{9}{2})(\frac{x}{\Delta})^3]v_l \end{aligned} \tag{20}$$

As before, the forces at the nodes i, j, k, and l can be related to the constants A_1, A_2, A_3, A_4 in the assumed σ_y in Eq. (19) as

$$\{F\} = [Q]\{A\} \tag{21}$$

where

$$\{F\} = \{F_{y_i} \quad F_{y_j} \quad F_{y_k} \quad F_{y_l}\}^T$$

$$\{A\} = \{A_1\sqrt{\Delta} \quad A_2\Delta \quad A_3\Delta^{3/2} \quad A_4\Delta^2\}$$

and

$$[Q] = -\frac{1}{840}\begin{bmatrix} 544 & 105 & 32 & 14 \\ 720 & 315 & 144 & 63 \\ 288 & 315 & 288 & 252 \\ 128 & 105 & 96 & 91 \end{bmatrix}$$

The strain-energy release rates are obtained by performing the integrations as in Eq. (11a) and using Eq. (21) as

$$G_I = -\frac{1}{2\Delta}\left[F_{y_i}(v_p - v_{p'}) + F_{y_j}(v_n - v_{n'}) + F_{y_k}(v_m - v_{m'})\right]$$

and (22)

$$G_{II} = -\frac{1}{2\Delta}\left[F_{x_i}(u_p - u_{p'}) + F_{x_j}(u_n - u_{n'}) + F_{x_k}(u_m - u_{m'})\right]$$

Note that the forces at node 1 do not appear in these equations because the relative displacement at node i is zero.

The strain-energy release rate formulas for this element are very similar to those of the linear and parabolic elements. The formulas given in Eq. (22) are also valid if triangular elements (Fig. 3(d)), obtained by collapsing one side of the cubic elements, are used at the crack tip.

Singularity Elements

Quarter-Point Singularity Element

Henshell and Shaw [3] and Barsoum [4] showed that square root singularities are produced at the crack tip if the midside nodes of an 8-noded element (Fig. 3(a)) are moved to the quarter-point positions as shown in Fig. 4(a). The quarter-point nodes

on the $y = 0$ line in this figure are nodes j and 1.

For this element, the σ_y distribution ahead of the crack tip on the $y = 0$ line is assumed to be like that given in Eq. (15). The shape functions of this element involve square root terms [4] and are

$$v(x) = \left(1 - 3\sqrt{\frac{x}{\Delta}} + 2\frac{x}{\Delta}\right)v_i + \left(4\sqrt{\frac{x}{\Delta}} - 4\frac{x}{\Delta}\right)v_j + \left(-\sqrt{\frac{x}{\Delta}} + 2\frac{x}{\Delta}\right)v_k \tag{23}$$

Using this shape function, the forces at the nodes i, j, and k can be related to the constants A_1, A_2, and A_3 of the assumed σ_y distribution of Eq. (15) as

$$\{F\} = [Q]\{A\} \tag{24}$$

where $\{F\}$ and $\{A\}$ are defined in Eq. (17), and

$$[Q] = -\frac{1}{30}\begin{bmatrix} 10 & 0 & -1 \\ 40 & 20 & 12 \\ 10 & 10 & 9 \end{bmatrix}$$

For non-singular elements the inversion of the matrix $[Q]$ was not necessary to determine $\{A\}$. However, for the singular elements this was not the case. The constants A_1, A_2, and A_3 are related to the nodal forces through

$$\{A\} = [Q]^{-1}\{F\} \tag{25}$$

where

$$[Q]^{-1} = -\frac{1}{4}\begin{bmatrix} 18 & -3 & 6 \\ -72 & 30 & -48 \\ 60 & -30 & 60 \end{bmatrix}$$

The strain-energy release rates were obtained by performing the integrations as in Eq. (11a) and using Eq. (25).

$$\begin{aligned} G_I = -\frac{1}{2\Delta} \; [& F_{y_i}\{t_{11}(v_m - v_{m'}) + t_{12}(v_1 - v_{1'})\} \\ & + F_{y_j}\{t_{21}(v_m - v_{m'}) + t_{22}(v_1 - v_{1'})\} \\ & + F_{y_k}\{t_{31}(v_m - v_{m'}) + t_{32}(v_1 - v_{1'})\}] \end{aligned} \tag{26a}$$

where

$$\begin{aligned} t_{11} &= 14 - \frac{33\pi}{8} \; ; \; t_{12} = -52 + \frac{33\pi}{2} \\ t_{21} &= -\frac{7}{2} + \frac{21\pi}{16} \; ; \; t_{22} = 17 - \frac{21\pi}{4} \\ t_{31} &= 8 - \frac{21\pi}{8} \; ; \; t_{32} = -32 + \frac{21\pi}{2} \end{aligned} \tag{26b}$$

A similar equation was obtained for G_{II}, where F_y is replaced with F_x and v is replaced with u.

In contrast to the regular parabolic elements, the strain-energy release rate equations for quarter-point (QP) elements have cross terms involving the corner and quarter-point forces and the relative displacements at the corner and quarter-point nodes. As before, the formulas given in Eq. (26) are also valid if triangular quarter-point elements (Fig. 4(b)), obtained by collapsing one side of the QP elements, are used at the crack

tip.

Cubic Singularity Element

Pu et al. [11] showed that a 12-noded cubic element has a square root singularity if the two side nodes are moved from the 1/3 and 2/3 positions to the 1/9 and 4/9 positions, respectively (see Fig. 4(c)). This is analogous to moving the midside nodes to the quarter points for a parabolic element. For this cubic singularity element, the same procedure as above was applied to obtain the strain-energy release rate equations.

For this element, the σ_y distribution ahead of the crack tip on the $y = 0$ line is assumed to be as given in Eq. (19). The shape functions of this element, as is the case for the quarter-point element, involve square root terms [11] and are

$$\begin{aligned} v(x) = {} & \left[1 - \frac{11}{2}\sqrt{\frac{x}{\Delta}} + 9\frac{x}{\Delta} - \frac{9}{2}\left(\frac{x}{\Delta}\right)^{3/2}\right]v_i \\ & + \left[9\sqrt{\frac{x}{\Delta}} - \frac{45}{2}\frac{x}{\Delta} + \frac{27}{2}\left(\frac{x}{\Delta}\right)^{3/2}\right]v_j \\ & + \left[-\frac{9}{2}\sqrt{\frac{x}{\Delta}} + 18\frac{x}{\Delta} - \frac{27}{2}\left(\frac{x}{\Delta}\right)^{3/2}\right]v_k \\ & + \left[\sqrt{\frac{x}{\Delta}} - \frac{9}{2}\frac{x}{\Delta} + \frac{9}{2}\left(\frac{x}{\Delta}\right)^{3/2}\right]v_l \end{aligned} \tag{27}$$

With these shape functions, the forces at the nodes i, j, k, and l can be related to the constants A_1, A_2, A_3, and A_4 of the assumed σ_y distribution in Eq. (19) as

$$\{F\} = [Q]\{A\} \tag{28}$$

where $\{F\}$ and $\{A\}$ were defined in Eq. (21), and the new

transformation matrix [Q] is

$$[Q] = -\frac{1}{420}\begin{bmatrix} 105 & 14 & 7 & 6 \\ 315 & 63 & 0 & -18 \\ 315 & 252 & 189 & 144 \\ 105 & 91 & 84 & 78 \end{bmatrix}$$

The constants (A) can be related to nodal forces as

$$(A) = [Q]^{-1}(F) \tag{29}$$

where

$$[Q]^{-1} = -\frac{1}{27}\begin{bmatrix} 216 & -34 & 16 & -54 \\ -1620 & 570 & -300 & 810 \\ 3240 & -1290 & 1020 & -2430 \\ -1890 & 770 & -770 & 1890 \end{bmatrix}$$

The strain-energy release rate equations were again obtained by performing the integrations as in Eq. (11(a)) and using Eq. (29) as

$$\begin{aligned} G_I = -\frac{1}{2\Delta}\frac{1}{54}\Big[& F_{y_i}\left(t_{11}(v_p - v_{p'}) + t_{12}(v_n - v_{n'}) + t_{13}(v_m - v_{m'})\right) \\ & + F_{y_j}\left(t_{21}(v_p - v_{p'}) + t_{22}(v_n - v_{n'}) + t_{23}(v_m - v_{m'})\right) \\ & + F_{y_k}\left(t_{31}(v_p - v_{p'}) + t_{32}(v_n - v_{n'}) + t_{33}(v_m - v_{m'})\right) \\ & + F_{y_l}\left(t_{41}(v_p - v_{p'}) + t_{42}(v_n - v_{n'}) + t_{43}(v_m - v_{m'})\right)\Big] \end{aligned} \tag{30a}$$

where

$$
\begin{aligned}
t_{11} &= -11187 + \frac{7155}{2}\pi \\
t_{12} &= 38556 - \frac{24543}{2}\pi \\
t_{13} &= -53055 + \frac{33777}{2}\pi \\
t_{21} &= \frac{11396}{3} - \frac{9575}{8}\pi \\
t_{22} &= -12936 + \frac{33003}{8}\pi \\
t_{23} &= 17988 - \frac{45837}{8}\pi \\
t_{31} &= -\frac{8453}{3} + \frac{3595}{4}\pi \\
t_{32} &= 9804 - \frac{12411}{4}\pi \\
t_{33} &= -13587 + \frac{17289}{4}\pi \\
t_{41} &= 6948 - \frac{17685}{8}\pi \\
t_{42} &= -23976 + \frac{60993}{8}\pi \\
t_{43} &= 33372 - \frac{84807}{8}\pi
\end{aligned}
\tag{30b}
$$

A similar equation was obtained for G_{II} where F_y is replaced with F_x and v is replaced with u. As before these formulas are applicable to triangular cubic elements (Fig. 4(d)) obtained by collapsing one side of the cubic singularity elements.

Mixed Mode Formulation

The G formulas presented earlier apply for pure mode I and for pure mode II problems. In mode I (or mode II) problems with

parabolic elements, the force F_{y_k} (or F_{x_k}), at node k from element J (see Figs. 3a and 4a) is exactly equal in magnitude but of the opposite (or same) sign to the force computed from the element J', the symmetric element about the x-axis. In mixed mode problems, the deformation is neither symmetric or antisymmetric about the x-axis (or the crack line). Therefore, even if the finite element model is symmetric about the crack line, as shown in Fig. 5, the forces $F_{y_k}^T$ and $F_{y_k}^B$ will not be equal in magnitude and opposite in sign to each other. (See the appendix for details.) Because the force F_{y_k} for the regular parabolic element and F_{y_1} for the regular cubic element (see Fig. 3) do not contribute to G, the formulas given for these elements in Eqs. (18) and (22) are also valid for mixed mode conditions.

However, the G formulas for the singularity element (Eqs. (26) and (30)) need to be modified for mixed mode conditions. The modification is necessary because, for quarter-point singularity elements, the nodal forces at node k have products involving the displacements at nodes l and m (see Fig. 4(a) and Eq. (26)). Similarly, for the cubic singularity elements, the nodal forces at node 1 have products involving displacements at nodes m, n, and p (see Eq. (30) and Fig. 4(c)). The required modifications are explained below.

In mixed mode conditions, the upper and lower crack faces do not deform symmetrically or antisymmetrically with respect to the crack tip. To close each of the crack faces from $a+\Delta$ to a,

different amounts of work are needed. The amount of work needed to close each crack surface can be found by computing the relative displacements of nodes on the crack surfaces relative to the crack tip and using the procedure outlined earlier.

The G formula for the quarter point element, then, is

$$G_I = -\frac{1}{2\Delta}\left[F_{y_i}\{t_{11}(v_m - v_{m'}) + t_{12}(v_1 - v_{1'})\}\right.$$
$$+ F_{y_j}\{t_{21}(v_m - v_{m'}) + t_{22}(v_1 - v_{1'})\}$$
$$\left. + F^T_{y_k}\{t_{31}\bar{v}_m + t_{32}\bar{v}_1\} + F^B_{y_k}\{t_{31}\bar{v}_{m'} + t_{32}\bar{v}_{1'}\}\right] \tag{31}$$

where $t_{11}, t_{12}, \ldots t_{32}$ are defined in Eq. (26b). $\bar{v}_m$ and $\bar{v}_{m'}$ are the relative displacements of nodes m and m', respectively, with reference to the crack tip node i: $\bar{v}_m = v_m - v_i$ and $\bar{v}_{m'} = v_{m'} - v_i$. The forces $F^T_{y_k}$ and $F^B_{y_k}$ are the forces computed from the elements J and J', respectively (see Fig. 5).

A similar equation was obtained for G_{II} where F_y is replaced with F_x and v is replaced with u. For pure mode I (or mode II) conditions, $F^B_{y_k} = -F^T_{y_k}$ and $F^B_{x_k} = F^T_{x_k}$ (or $F^B_{y_k} = F^T_{y_k}$ and $F^B_{x_k} = -F^T_{x_k}$), and Eq. (31) reduces to Eq. (26).

For mixed mode conditions, the G formula for the cubic singularity element is

$$
\begin{aligned}
G_I = -\frac{1}{2\Delta}\frac{1}{54}\Big[& F_{y_i}\{t_{11}(v_p - v_{p'}) + t_{12}(v_n - v_{n'}) + t_{13}(v_m - v_{m'})\} \\
& + F_{y_j}\{t_{21}(v_p - v_{p'}) + t_{22}(v_n - v_{n'}) + t_{23}(v_m - v_{m'})\} \\
& + F_{y_k}\{t_{31}(v_p - v_{p'}) + t_{32}(v_n - v_{n'}) + t_{33}(v_m - v_{m'})\} \\
& + F^T_{y_1}\{t_{41}\bar{v}_p + t_{42}\bar{v}_n + t_{43}\bar{v}_m\} \\
& + F^B_{y_1}\{t_{41}\bar{v}_{p'} + t_{42}\bar{v}_{n'} + t_{43}\bar{v}_{m'}\}\Big]
\end{aligned}
\tag{32}
$$

where $t_{11}, t_{12}, \ldots, t_{43}$ are defined in Eq. (30b). The forces $F^T_{y_1}$ and $F^B_{y_1}$ are the forces in the y-direction computed from elements J and J', respectively (see Fig. 5).

A similar equation for G_{II} is obtained where F_y is replaced with F_x and v is replaced with u. For pure mode I or mode II cases, Eq. (32) reduces to Eq. (30).

SIMPLIFIED G FORMULAS FOR SINGULARITY ELEMENTS

The G formulas for the non-singular elements, Eqs. (13), (14), (18), and (22), are simple. In contrast, the formulas for the singularity elements are awkward, even for pure mode I or pure mode II conditions. The formulas are even more complicated for mixed mode conditions. The complexity of these formulas can be traced to the terms involving the forces at node k for the QP elements (Eqs. (26) and (31)), and at node 1 for the cubic singularity elements (Eqs. (30) and (32)). The G formulas can be simplified considerably if these forces can be approximated.

For the QP element, three constants A_1, A_2, and A_3 were

assumed in the σ_y distribution (Eq. (15)) because the three forces at nodes i, j, and k (Fig.4) were used. However, if only two constants A_1 and A_2 are retained in the σ_y distribution, only the forces at nodes i and j are needed to evaluate these constants. This assumption requires the forces at node k to be dependent on the forces at nodes i and j, and will simplify the formulas considerably. Setting the constant A_3 to zero in Eq. (25) yields

$$F_{y_k} = - F_{y_i} + \frac{1}{2} F_{y_j} \tag{33}$$

Substitution of this value of F_{y_k} into Eq. (26) or (31) gives

$$\begin{aligned} G_I = - \frac{1}{2\Delta} \; [& F_{y_i} (t_{11}(v_m - v_{m'}) + t_{12}(v_1 - v_{1'})) \\ & + F_{y_j} (t_{21}(v_m - v_{m'}) + t_{22}(v_1 - v_{1'}))] \end{aligned} \tag{34a}$$

where

$$\begin{aligned} t_{11} &= 6 - \frac{3\pi}{2} \; ; \; t_{12} = 6\pi - 20 \\ t_{21} &= \frac{1}{2} \; ; \; t_{22} = 1 \end{aligned} \tag{34b}$$

A similar equation was obtained for G_{II} where F_y is replaced with F_x and v is replaced with u. Note that this equation is valid for pure mode I, mode II, and mixed mode conditions. This equation is considerably simpler and easier to use than either Eq. (26) or Eq. (31).

A similar procedure can be followed for the cubic singularity elements. In this case, only three constants are used in the expression for σ_y. Setting constant A_4 to zero in

Eq. (29) yields

$$F_{y_1} = F_{y_i} - \frac{11}{27} F_{y_j} + \frac{11}{27} F_{y_k} \tag{35}$$

Substitution of this expression for F_{y_1} into Eqs. (30) and (32) gives

$$\begin{aligned} G_I = -\frac{1}{2\Delta}[&F_{y_i}\{t_{11}(v_p - v_{p'}) + t_{12}(v_m - v_{m'}) + t_{13}(v_n - v_{n'})\} \\ &+ F_{y_j}\{t_{21}(v_p - v_{p'}) + t_{22}(v_m - v_{m'}) + t_{23}(v_n - v_{n'})\} \\ &+ F_{y_k}\{t_{31}(v_p - v_{p'}) + t_{32}(v_m - v_{m'}) + t_{33}(v_n - v_{n'})\}] \end{aligned} \tag{36a}$$

where

$$\begin{aligned} t_{11} &= -\frac{157}{2} + \frac{405}{16}\pi \\ t_{12} &= 270 - \frac{1377}{16}\pi \\ t_{13} &= -\frac{729}{2} + \frac{1863}{16}\pi \\ t_{21} &= \frac{484}{27} - \frac{395}{32}\pi \\ t_{22} &= -\frac{176}{3} + \frac{151}{8}\pi \\ t_{23} &= \frac{244}{3} - \frac{209}{8}\pi \\ t_{31} &= \frac{13}{54} - \frac{5}{144}\pi \\ t_{32} &= \frac{2}{3} + \frac{\pi}{16} \\ t_{33} &= \frac{1}{6} + \frac{1}{16}\pi \end{aligned} \tag{36b}$$

A similar equation was obtained for G_{II} where F_y is replaced with F_x and v is replaced with u. Again, this equation is valid for pure mode I, mode II, and mixed mode conditions, and is considerably simpler and easier to use than either Eq. (30) or

Eq. (32).

Eqs. (26), (30), (31), and (32) will be referred to as the consistent formulas. Eqs. (34) and (36) will be referred to as the simpler formulas. The accuracy of the consistent and simpler formulas will be studied later in this paper by applying the formulas to two mode I and two mixed mode problems for which reference solutions are available.

MODIFICATION FOR PRESSURE LOADED CRACK FACES

The procedure developed earlier is valid for calculating strain-energy release rates for self-similar crack growth when the crack faces are stress free. When the crack faces are pressure loaded, the procedure outlined above must be modified. To illustrate this modification, consider a central crack of length 2a in an infinite plate.

Figure 6 shows the region very near the crack tip with a uniform pressure loading of magnitude S applied to crack faces. As before, the strain-energy release rate is related to the work required to close the crack from $a + \Delta$ to a. The closure of the crack faces from $a + \Delta$ to a can be divided into two parts. In the first part, the applied pressure between $a + \Delta$ and a is erased and, in the second part, the stress free crack faces between $a + \Delta$ and a are closed. In the finite element analysis, the first part is equivalent to addition of nodal forces consistent to the opposite of the applied pressure at all nodes between $a + \Delta$ and a. For the second part, the general

procedure described earlier is used.

For a regular 8-noded element, the uniform pressure S acting between $a + \Delta$ and a translates into three consistent nodal forces of values $\frac{S}{6}\Delta$, $\frac{2S}{3}\Delta$, and $\frac{S}{6}\Delta$ acting at nodes i, j, and k respectively (see Fig. 6). To erase this pressure, the opposites of these forces are applied to nodes i, j, and k as shown in Fig. 6(b), and added to the finite element computed forces $F^c_{y_i}$, $F^c_{y_j}$, and $F^c_{y_k}$ at nodes i, j, and k, respectively, (see Fig. 6(b)). Thus, the forces at nodes i, j, and k, to be used in Eq. (18), will be

$$\begin{aligned} F_{y_i} &= F^c_{y_i} - \frac{S}{6}\Delta \\ F_{y_j} &= F^c_{y_j} - \frac{2S}{3}\Delta \\ F_{y_k} &= F^c_{y_k} - \frac{S}{6}\Delta \end{aligned} \tag{37}$$

Eqs. (37) show that the correct forces to be used in the G calculations for a crack face loading are sum of the computed finite element forces and the negative of the consistent nodal forces for the pressure distribution. The consistent nodal forces for an uniform pressure distribution of magnitude S for the various elements considered in this paper are shown in Fig. 7. These forces are then added to the forces computed at the nodes. The corrected forces, F_{y_i}, F_{y_j}, etc., are then used in

the appropriate G equations presented earlier to calculate the strain-energy release rates.

EVALUATION OF G FORMULAS

The formulas presented in this paper are used to calculate strain-energy release rates for cracks in two mode I and two mixed mode problems. The results are compared to those from the literature. The percent error is defined here as

$$\text{Percent error} = \frac{\text{Present result} - \text{Reference result}}{\text{Reference result}} * 100$$

Unless otherwise specified, a Poisson's ratio of 0.3 was used for all configurations analyzed.

In all the problems studied, the finite element idealization at the crack tip had triangular elements with straight sides. These elements were obtained by collapsing one side of the parabolic or cubic elements. These triangular elements are preferred over their rectangular or curved counterparts as suggested in Refs. 4, 11, 18, and 19.

Mode I Problems

Remote Loading

Center-cracked tension specimen. - The first example is a center cracked tension (CCT) specimen with a crack-length-to-width ratio of 0.8 (see Fig. 8(a)). From the symmetries in the problem, only one-quarter of the specimen was analyzed. Fig.

8(c) shows the finite element idealization for the 8-noded parabolic elements and the 12-noded cubic elements. The specimen was analyzed four ways: (1) regular parabolic elements everywhere, (2) regular parabolic elements with QP elements at the crack-tip, (3) cubic elements everywhere, and (4) cubic elements with cubic singularity elements at the crack tip. For each case, the strain-energy release rates were obtained using the formulas presented earlier. Table 1 presents the normalized forces and crack opening displacements (COD), and the strain-energy release rates. The four G values are within about 3 percent of an accurate value from Ref. 20. The models with the singularity elements, as expected, yielded the most accurate results. For these cases, both of the simpler formulas yielded G values which are more accurate than their consistent counterparts.

Single edge notched specimen. - The second example was a single edge notched specimen with a/b = 0.8 (Fig. 8(b)). Again the finite element idealization of Fig. 8(c) was used. Table 2 presents the normalized forces, COD, and the strain-energy release rates obtained for all 4 idealizations. The strain-energy release rates obtained were generally about 6% lower than an accurate solution given in Ref. 20. Again the models using the singularity elements yielded more accurate G values than the models using the non-singular elements. As in the CCT case, the simpler formulas yielded G values which are more accurate than their consistent counterparts.

Crack Face Loading

As pointed earlier, the forces used in the G formulas must be modified for loaded crack faces (see Eq. (37)). To verify this modification, a center cracked plate with crack-face pressure loading was analyzed. Table 3 presents the forces on the nodes at and ahead of the crack tip obtained from the finite element analysis for the QP and cubic singularity elements. This table also presents the forces used in the G calculations. Because the stress-intensity factors and strain-energy release rates are identical for crack-face loading and remote loading, the COD should be identical for these two loadings. Therefore, the modified forces in column 4 of Table 3 should be identical to those obtained with the remote loading. A comparison of column 4 of Table 3 and column 2 of Table 1 shows that this is true. This verifies the modification outlined earlier for the crack face pressure loading.

Mixed Mode Problems

To evaluate the accuracy of the formulas for mixed mode problems, an angle crack problem and a cracked interface problem were analyzed. The calculated strain-energy release rates are compared to those from the literature.

Angle Crack

Fig. 9(a) shows the configuration used for the angle crack in a finite plate. Fig. 10(a) and (b) present the finite element

idealizations with 8-noded parabolic elements and 12-noded cubic elements, respectively. Fig. 10(c) shows the details at the crack tip. With the parabolic elements, quarter point singularity elements with $\Delta = 0.04a$ were used at the crack tip. In the cubic element model, cubic singularity elements with $\Delta = 0.045a$ were used at the crack tip.

Fig. 11 shows the forces at the crack tip. The forces at nodes i, j, and k and the displacements at nodes m and 1 are needed to compute G. These forces and displacements, represented as components that are normal and tangential to the crack plane, can be computed as follows. First, the Cartesian forces F_x and F_y at nodes i, j, and k are obtained. At node i (Fig. 10), the forces F_{x_i} and F_{y_i} can be computed from elements I, J, K, and L. The forces F_{x_j}, F_{y_j}, F_{x_k}, and F_{y_k} can be computed from element L alone. The tangential and normal forces at the crack tip, F_{t_i} and F_{n_i}, can be computed as

$$\begin{aligned} F_{t_i} &= F_{x_i} \cos\theta + F_{y_i} \sin\theta \\ F_{n_i} &= -F_{x_i} \sin\theta + F_{y_i} \cos\theta \end{aligned} \tag{38}$$

with similar equations for the forces at nodes j and k. Similarly, the normal and tangential displacements at nodes m, m', 1, and 1' relative to the crack tip can be computed by

first calculating the Cartesian relative displacements as

$$\bar{u}_m = u_m - u_i$$
$$\bar{v}_m = v_m - v_i \qquad (39)$$

A similar set of equations were used for nodes m', 1, and 1'. The normal and tangential forces and displacements are then used to obtain the G_I and G_{II} values.

Table 4 presents the G_I and G_{II} values obtained with quarter-point and cubic singularity elements. For comparison, this table also contains the results from Wilson's collocation procedure [21] and Tan et al.'s boundary force method [22].

In view of the slight (2 percent) difference between the collocation and boundary force method results, the present results are compared with the average of these reference results. The present results are in good agreement with the reference results. The accuracy is better for mode I than for mode II. Again the differences between the simpler and consistent formulas are negligible.

Cracked Bimaterial Plate

The second mixed mode problem analyzed was a bimaterial plate with a central crack along the interface (Fig. 9(b)). Erdogan and Gupta [23] analyzed this problem for an infinite plate with uniform pressure applied to the crack faces. Their calculated G values will be used to evaluate the present

results.

Because of symmetry, only one-half of the plate was idealized, as shown in Fig. 12(a). Fig. 12 shows the finite element model using 8-noded parabolic and QP singularity elements. Table 5 presents the strain-energy release rates obtained using Eqs. (31) and (34) for three sets of material combinations. The strain-energy release rates given in Ref. 23 were divided by a factor 2 because Erdogan and Gupta's definition of G was different from the classical definition (see Eq. (37) on p. 1097 of Ref. 23). Excellent agreement is obtained between the finite element computations and those of reference 23.

In this bimaterial case the power of the stress singularity at the crack tip is of the form $-1/2 \pm i\alpha$, where α depends on the relative properties of the two materials. This indicates that the stresses oscillate near the crack tip. The solution in Ref. 23 includes the oscillatory part of the stresses. In the present finite element analysis, however, this oscillatory behavior is neglected. The accuracy of the present results show that contribution of the oscillatory part to the strain-energy release rate is negligible.

CONCLUDING REMARKS

A general procedure is presented for obtaining the strain-energy release rate G for cracks using the virtual crack-closure technique in finite element analyses. The procedure was applied to non-singular 4-noded, 8-noded (parabolic), and 12-

noded (cubic) elements and then to quarter-point and cubic singularity elements. The procedure assumes that the finite element idealization is symmetric about the crack plane at the crack tip and symmetric about a line normal to the crack plane at the crack tip. The procedure uses forces at and ahead of the crack tip and displacements behind the crack tip. With this procedure, simple formulas were obtained for the non-singular elements.

For the singularity elements, two types of formulas - consistent and simpler - were obtained. The consistent formulas use three nodal forces for the quarter-point singularity element, and four nodal forces for the cubic singularity elements. In contrast, the simpler formulas use two and three nodal forces for the quarter-point and cubic singularity elements, respectively.

A slight modification was necessary to use the formulas when the crack faces were subjected to pressure loading. The finite element forces need to be modified to account for the pressure loading. The modification is simple, accurate and is easy to implement in the actual analysis.

Two mode I and two mixed mode problems were analyzed using the non-singular and singular elements mentioned above. The strain-energy release rates for these problems were obtained using the formulas derived in this paper. Comparisons with accurate or reference solutions from the literature showed that, for the configurations analyzed, the G formulas yielded accurate results. For all the configuration analyzed, the simpler

formulas for the singularity elements yielded strain-energy release rates which were more accurate than their consistent counterparts.

With the singularity elements, fewer elements (and, hence, fewer degrees of freedom) are needed to obtain accurate solutions. The simpler strain-energy release rate formulas developed in this paper for singularity elements considerably simplified the G formulas without sacrificing accuracy. These formulas will enhance the utility of these elements in the analysis of cracked isotropic and bimaterial configurations.

The analysis and procedure presented in this paper should provide the basis for future development of formulas for strain-energy release rates for cracked orthotropic and anisotropic materials.

Acknowledgements

The procedure presented in this paper came out of discussions with Dr. J. H. Crews, Jr. of the Materials Division, NASA Langley Research Center, Hampton, VA. The author takes this opportunity to thank him for many helpful discussions. This work was performed at the Langley Research Center as part of NASA Contracts NAS1-17808 and NAS1-18256.

Appendix
Inequality of Forces at Node k

This appendix will show that the forces at node k (see Fig. 5(b)) computed from the elements J and J′ will not be the same for mixed mode conditions.

A mixed mode condition can be thought of as the superposition of mode I and mode II conditions. Fig. 13 shows the forces at node k computed from elements J and J′ for mode I, mode II, and mixed mode conditions. For the mode I (mode II) case, symmetry (antisymmetry) conditions about the y = 0 line require that the x- and y-forces be symmetric (antisymmetric). Note that the forces F_x^I for mode I and F_y^{II} for mode II will not, in general, be equal to zero. (The requirement of a zero x-force at node k for mode I and a zero y-force at node k for mode II can still be satisfied because elements to the right of elements J and J′ contribute to these forces.)

Superposition of the forces at node k from the mode I and mode II conditions will yield the forces for the mixed mode case as shown in Fig. 13. The y-force at node k from element J is $F_y^I + F_y^{II}$ while that from element J′ is $-F_y^I + F_y^{II}$. Similarly, the x-force at node k from element J is $F_x^I + F_x^{II}$ and that from element J′ is $F_x^I - F_x^{II}$. Thus, the forces at node k

computed from the top and bottom elements will not be equal. Similar arguments hold for node 1 in Fig. 5(c).

REFERENCES

1. Rooke, D. P., Baratta, F. I, and Cartwright, D. J., "Simple methods of determining stress-intensity factors," Engineering Fracture Mechanics, Vol. 14, 1981, pp. 397-426.

2. Raju, I. S. and Newman, J. C., Jr., "Methods for analysis of cracks in three-dimensional solids," J. Ae. Soc of India, Special Issue on Fracture Mechanics, Vol. 36, No. 3, 1984, pp. 153-172.

3. Henshell, R. D. and Shaw, K. G., "Crack tip finite elements are unnecessary," Int. Jnl. of Numerical Methods in Engineering, Vol. 9, 1975, pp. 496-507.

4. Barsoum, R. S., "On the use of isoparametric finite elements in linear fracture mechanics," Int. Jnl. Of Numerical Methods in Engineering, Vol. 10, 1976, pp. 25-37.

5. Blackburn, W. S. and Hellen, T. K., "Calculation of stress-intensity factors in three-dimensions by finite element method," Int. Jnl. of Numerical Methods in engineering, Vol. 11, 1979, pp. 211-229.

6. O'Brien, T. K., "Characterization of delamination onset and growth in a composite laminate", Damage in Composite Materials, STP 775, American Society for Testing and Materials, Philadelphia, 1982, pp. 140-147; also in NASA TM-81940, Jan. 1981.

7. O'Brien, T. K., "Mixed mode strain-energy-release-rate effects on edge delamination of composites," The Effect of Defects in Composite Materials, STP 836, American Society for Testing and Materials, Philadelphia, 1984, pp. 125-142; also in NASA TM-84592, Jan. 1983.

8. Rybicki, E. F. and Kanninen, M. F., "A finite element calculation of stress-intensity factors by a modified crack closure integral," Engineering Fracture Mechanics, Vol. 9, 1977, pp. 931-938.

9. Parks, D. M., "A stiffness derivative finite element technique for determination of crack tip stress-intensity factors," Int. Jnl. of Fracture, Vol. 10, 1974, pp. 487-502.

10. Hellen, T. K., "On the method of virtual crack extensions," Int. Jnl. of Numerical Methods in Engineering, 1975, Vol. 9, pp. 187-207.

11. Pu, S. L., Hussain, M. A., and Lorensen, W. E., "The collapsed cubic isoparametric element as a singular element for crack problems," Int. Jnl. of Numerical Methods in Engineering, Vol. 12, 1978, pp. 1727-1742.

12. Atluri, S. N., Kobayashi, A. S., and Nakagaki, M., "An assumed displacement hybrid finite element model for linear fracture mechanics," Int. Jnl. of Fracture, Vol. 11, No. 2, 1975, pp. 257-271.

13. Whitcomb, J. D. and Raju, I. S., "Analysis of interlaminar stresses in thick composite laminates with and without edge delamination," Delamination and Debonding of Materials, ASTM STP 876, W. S. Johnson, Ed., American Society for Testing and Materials, Philadelphia, 1985, pp. 69-94.

14. Dattaguru, B., Everett, R. A., Jr., Whitcomb, J. D., and Johnson, W. S., "Geometrically nonlinear analysis of adhesively bonded joints," Journal of Engineering Materials and Technology, Vol. 106, Jan. 1984, pp. 59-65.

15. Whitcomb, J. D. and Dattaguru, B., "User's manual for GAMNAS -- geometric and material nonlinear analysis of structures," NASA TM-85734, Jan. 1984.

16. O'Brien, T. K., Raju, I. S., and Garber, D. P., "Residual thermal and moisture influences on the strain-energy release rate analysis of edge delamination", Jnl. of Composites, Technology & Research, Vol. 8, No. 2, Summer 1986, pp. 37-47.

17. Krishnamurthy, T., Ramamurthy, T. S., Vijayakumar, K., and Dattaguru, B., "Modified crack-closure integral method for higher order finite elements," Paper presented at FEICOM-5, Bombay, India, December 1985.

18. Barsoum, R. S., Discussion of a Paper by R. D. Henshell and K. G. Shaw, Int. Jnl. of Numerical Methods Engineering, Vol. 10, 1976, pp. 235-237.

19. Freese, C. E., and Tracey, D. M., "The natural isoparametric triangle versus collapsed quadrilateral for elastic crack analysis," Int. Jnl. Fracture, Vol. 12, 1976, pp. 767-770.

20. Tada, H., Paris, P. C. and Irwin, G. R., The Stress Analysis of Cracks Handbook, Del Research Corp., 1973.

21. Rooke, D. P. and Cartwright, D. J., Compendium of Stress-Intensity Factors, London, HMSO, 1976.

22. Tan, P. W., Raju, I. S., and Newman J. C., Jr, "Boundary force method for analyzing two-dimensional cracked bodies," NASA TM-87725, May 1986.

23. Erdogan, F. and Gupta, G. D. "Layered composites with an interface flaw," Int. Jnl. Solids and Structures, Vol. 7, 1971, pp. 1089-1107.

Table 1 - Comparison of strain-energy release rates for a center cracked tension specimen subjected to remote uniform stress S
(a/b= 0.8 ; Δ/a = 0.0625 ; plane strain)

$$G_{Reference}\ [20] = 3.298\ \frac{S^2 \pi\ a(1-\nu^2)}{E}$$

Element Used	Nodal Forces F_y/Sa		Relative Crack Opening Displacement Ev/Sa		$\frac{EG}{S^2\ \pi a(1-\nu^2)}$	Percent Error
Non-Singular Elements						
8-noded Parabolic Element (Fig. 3(a))	i	-0.3218	m	2.179	3.197	-3.0
	j	-0.2969	l	1.487		
12-noded Cubic Element (Fig. 3(c))	i	-0.2552	p	2.240	3.239	-1.8
	j	-0.2360	n	1.835		
	k	-0.1203	m	1.269		
Singularity Elements						
QP Singularity Element (Fig. 4(a))	i	-0.1068	m	2.276	3.242	-1.7
	j	-0.4348	l	1.156	(3.269)*	(-0.9)
	k	-0.0941				
Cubic Singularity Element (Fig 4(c))	i	-0.0806	p	2.292	3.271	-0.8
	j	-0.2406	n	1.544	(3.285)	(-0.4)
	k	-0.2471	m	0.7767		
	l	-0.0698				

*Values in parenthesis were obtained with simpler formulas.

Table 2 - Comparison of strain-energy release rates for a single edge notched specimen subjected to remote uniform stress S
(a/b = 0.8; Δ/a = 0.0625; plane strain)

$$G_{\text{Reference}}\ [20] = 143.8\ \frac{S^2 \pi a(1-\nu^2)}{E}$$

Element Used	Nodal Forces F_y/Sa				Relative Crack Opening Displacement Ev/Sa	$\frac{EG}{S^2 \pi a(1-\nu^2)}$	Percent Error
Non-Singular Element							
8-noded Parabolic Element (Fig. 3)	i	-1.985	m	15.95		128.9	-10.0
	j	-1.414	l	10.19			
12-noded Cubic Element (Fig. 3)	i	-1.602	p	16.74		134.6	-6.4
	j	-1.346	n	13.10			
	k	-0.4236	m	8.645			
Singularity Elements							
QP Singularity Element (Fig. 4)	i	-0.7192	m	17.08		134.8 (137.4)*	-6.5 (-4.5)
	j	-2.432	l	7.804			
	k	-0.2309					
Cubic Singularity Element (Fig. 4)	i	-0.5052	p	17.37		138.6 (139.0)	-3.7 (-3.3)
	j	-1.574	n	10.85			
	k	-1.163	m	5.191			
	l	-0.2596					

*Values in parenthesis were obtained with simpler formulas

Table 3 - Nodal forces for a center cracked tension specimen with uniform crack face loading of magnitude S

(a/b = 0.8; Δ/a = 0.0625; plane strain)

F_y/Sa

		Forces computed in the finite element analysis	Forces needed to erase the crack face loading	Forces to be used in the formula*
QP Element (Fig. 4)	i	-0.1068	0	-0.1068
	j	-0.3931	-0.0417	-0.4348
	k	-0.0733	-0.0208	-0.0941
Cubic Singularity Element (Fig. 4)	i	-0.0785	-0.0021	-0.0806
	j	-0.2312	-0.0094	-0.2406
	k	-0.2096	-0.0375	-0.2471
	l	-0.0562	-0.0135	-0.0698

*Forces in this column are identical to those computed with a remote uniform stress of magnitude S applied on the line y = h (see Fig. 8).

Table 4 - Comparison of strain-energy release rates for an angle crack in a finite plate ($a/b = 0.5$; $\phi = 45°$; plane strain)

Element Used	$\frac{EG_I}{S^2\pi a(1-\nu^2)}$	$\frac{EG_{II}}{S^2\pi a(1-\nu^2)}$
QP Singularity Element	1.436 (1.447)*	0.3378 (0.3399)
Cubic Singularity Element	1.433 (1.444)	0.3446 (0.3354)
Reference Results		
Wilson [21]+ (Collocation)	1.440	0.325
Tan et al. [22] (Boundary Force Method)	1.416	0.3295

*Values in parenthesis were obtained with simpler formulas.

+These values were taken from Figs. 60 and 61 of ref. 21

Table 5 - Comparison of strain-energy release rates for center crack along the interface in bimaterial plate with crack face pressure loading S (a/b = 0.1; plane strain)

$$\frac{E_1 G}{S^2 \pi a (1-\nu^2_1)}$$

Material 1	Material 2	Mode I	Mode II	Total	Total Ref [23]&	Percent Error
Aluminum	Epoxy	10.35	0.7262	11.08	10.92	1.42
		(10.43)	(0.6296)	(11.05)+		1.21
Steel	Epoxy	29.56	2.808	32.05	31.66	1.23
		(29.77)	(2.168)	(31.94)		0.88
Steel	Aluminum	1.934	-0.0567	1.877	1.980	-5.19
		(1.947)	(-0.0567)	(1.890)		-4.56

MATERIAL PROPERTIES

Material	E, psi	ν
Epoxy	$0.45 * 10^6$	0.35
Aluminum	$10 * 10^6$	0.3
Steel	$30 * 10^6$	0.3

+The total G values of reference [23] were scaled down by factor 2 because Erdogan and Gupta defined G for an isotropic, homogeneous plate as

$$G = 2 \frac{K^2_I}{E} (1-\nu^2)$$

&Values in parenthesis were obtained with simpler formulas.

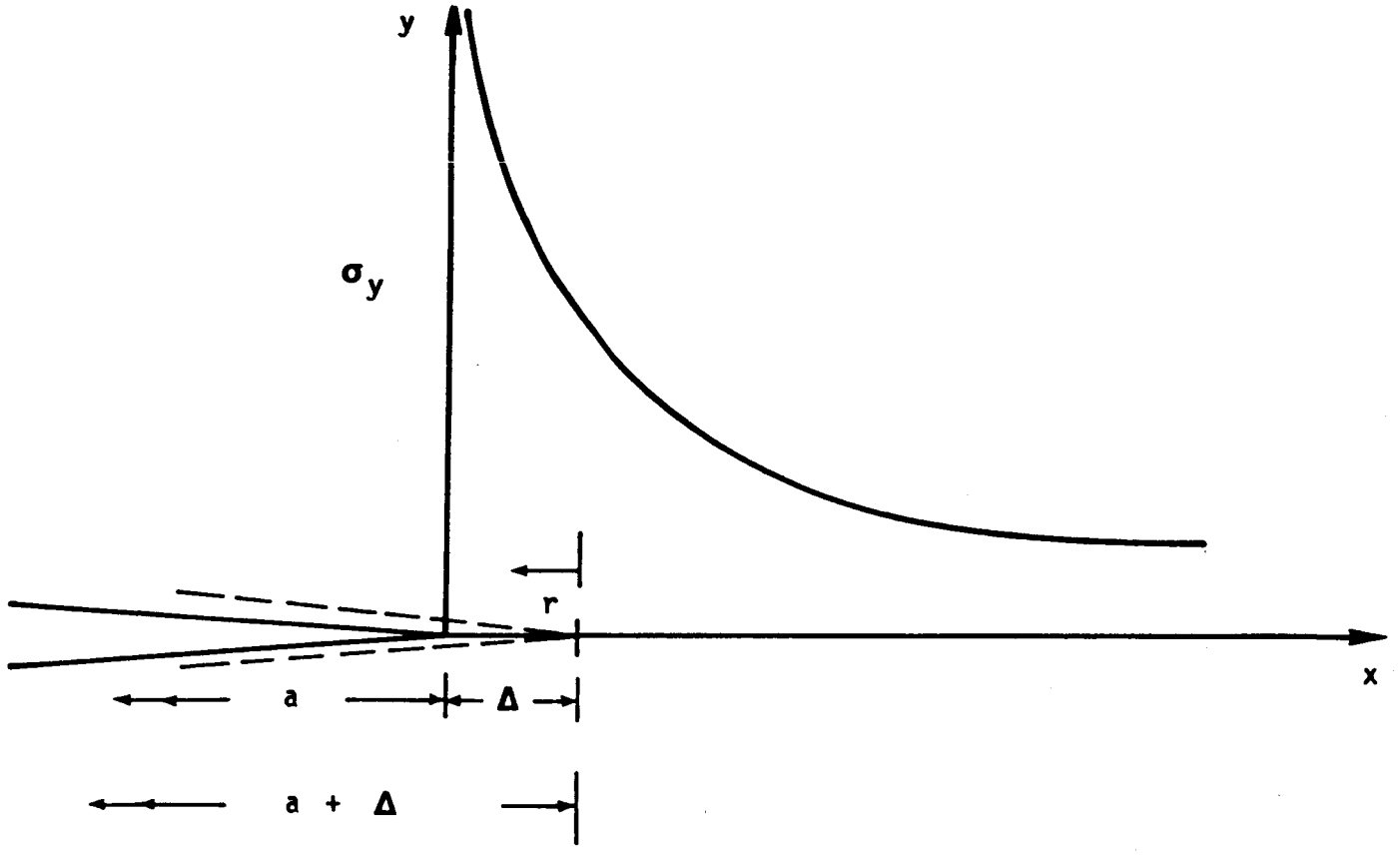

(a) Normal stress (σ_y) distribution ahead of the crack

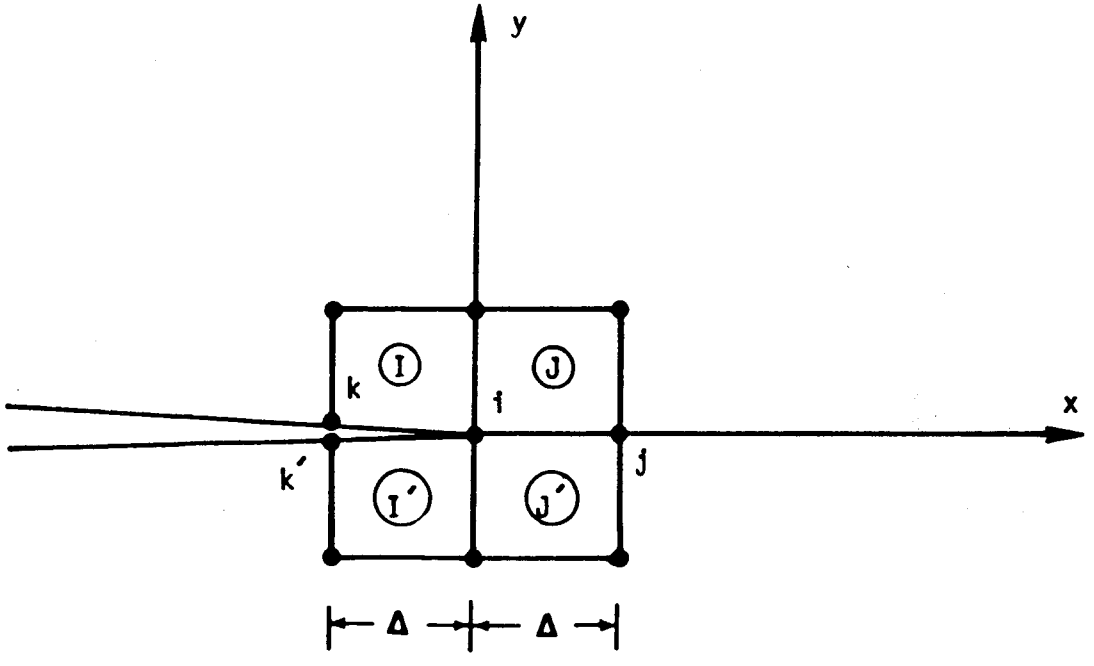

(b) Four 4-noded elements at the crack tip

Fig. 1: Irwin's virtual crack-closure method

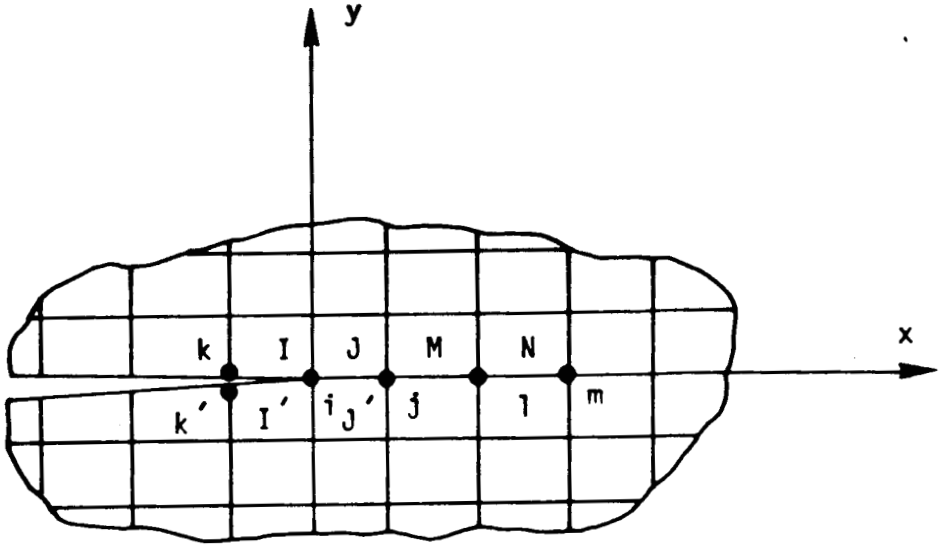

(a) Finite element idealization near the crack tip

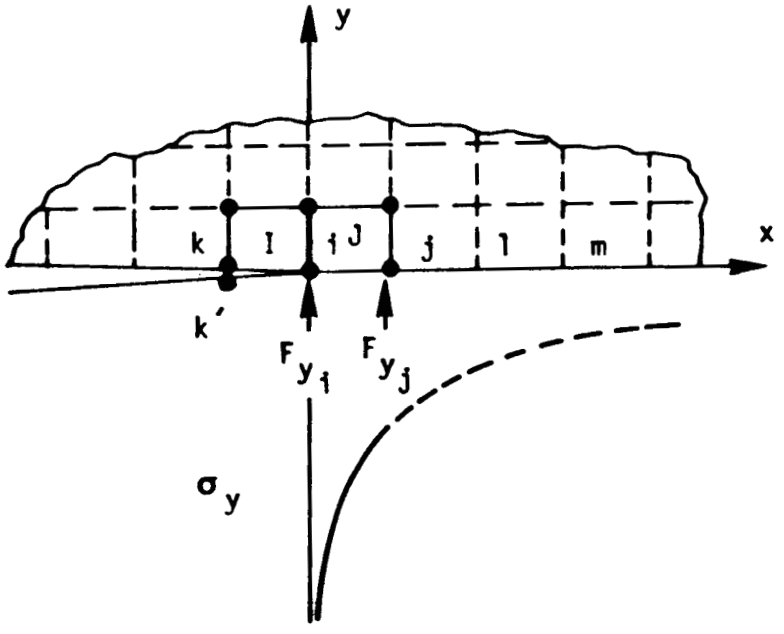

(b) Stress distribution and nodal forces

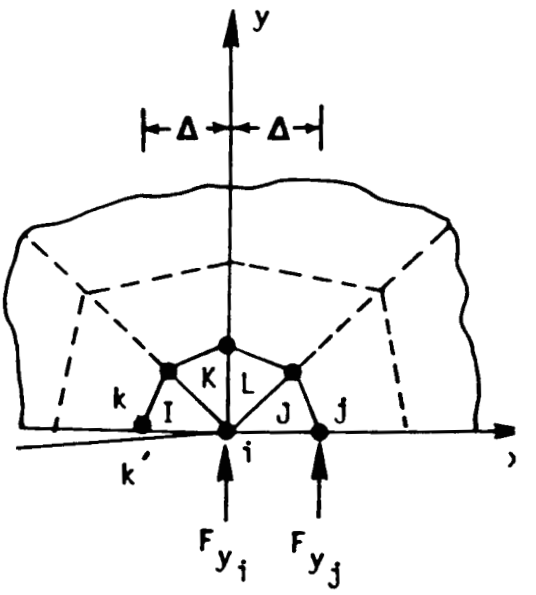

(c) Collapsed 4-noded elements at crack tip

Fig. 2: Normal Stress Distribution and Consistent Normal Forces

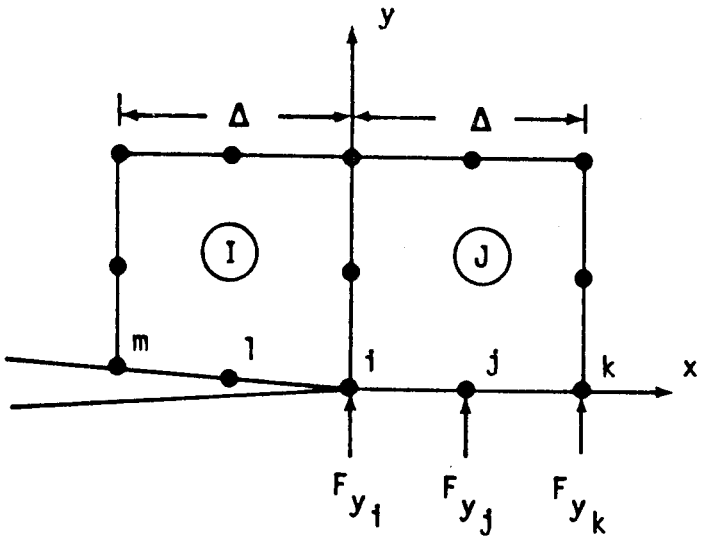

(a) 8-noded parabolic element

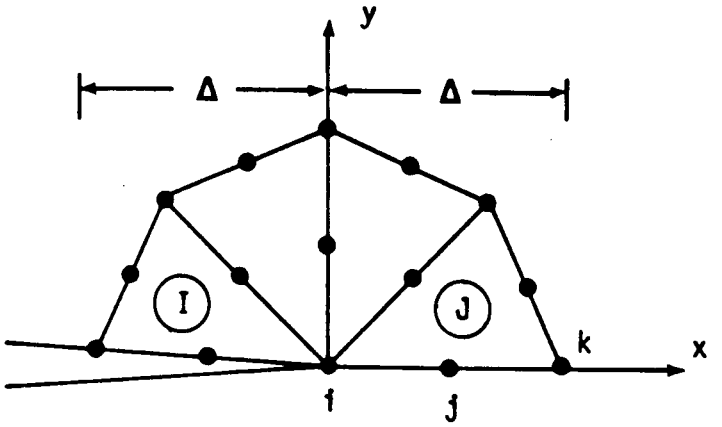

(b) Collapsed Parabolic element

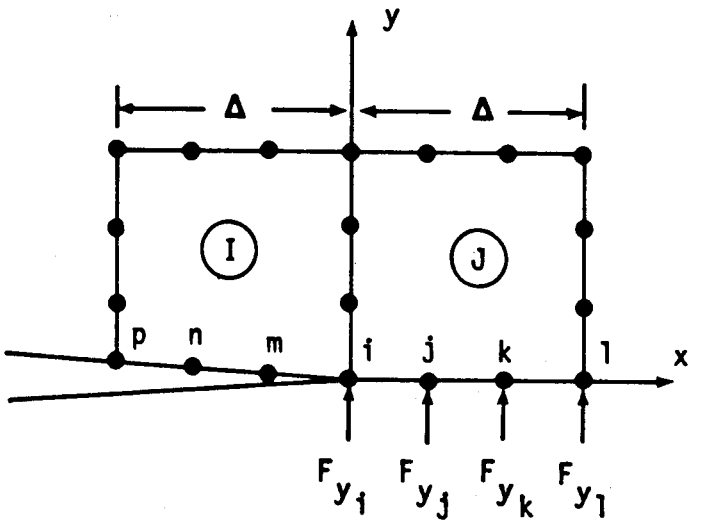

(c) 12-noded cubic element

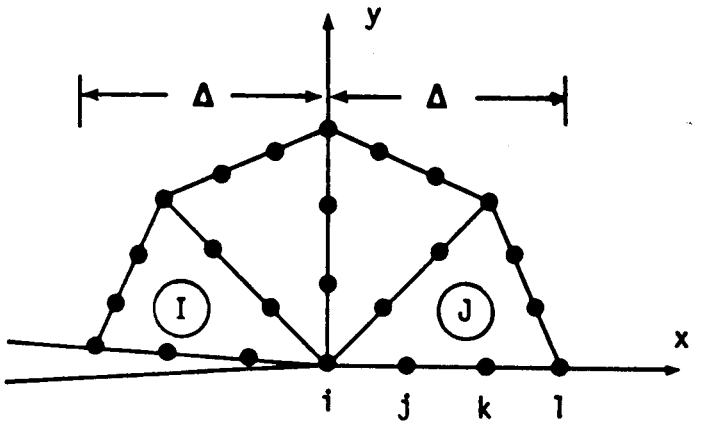

(d) Collapsed cubic element

Fig. 3 - Non-singular elements

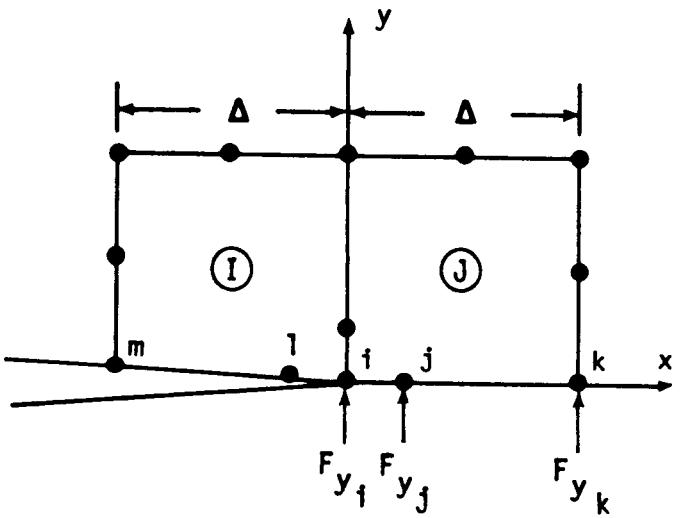

(a) Rectangular QP elements

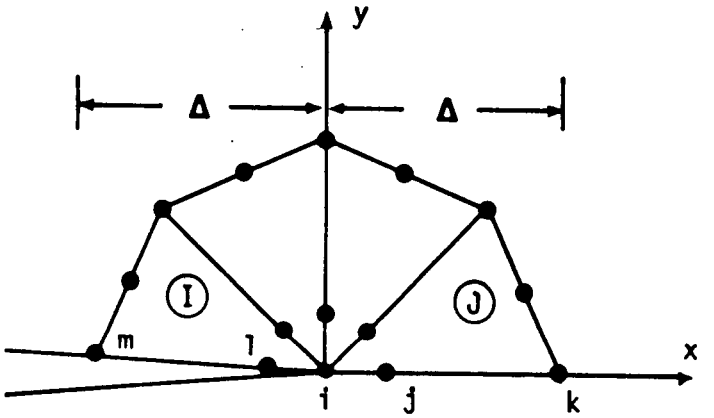

(b) Collapsed QP element

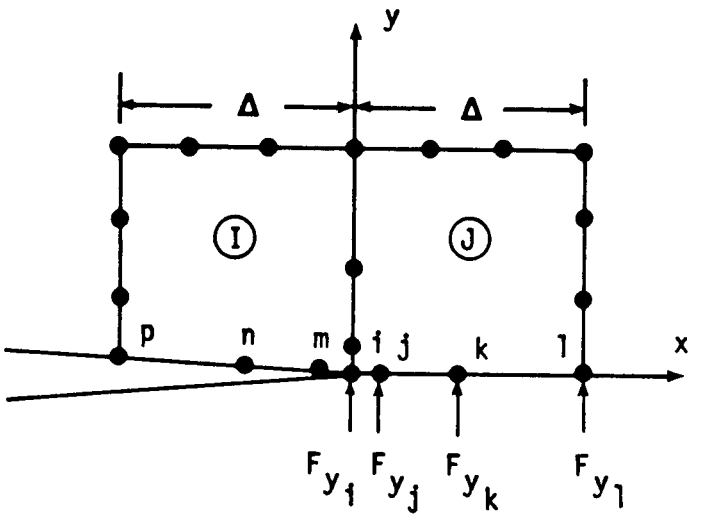

(c) Rectangular cubic singularity element

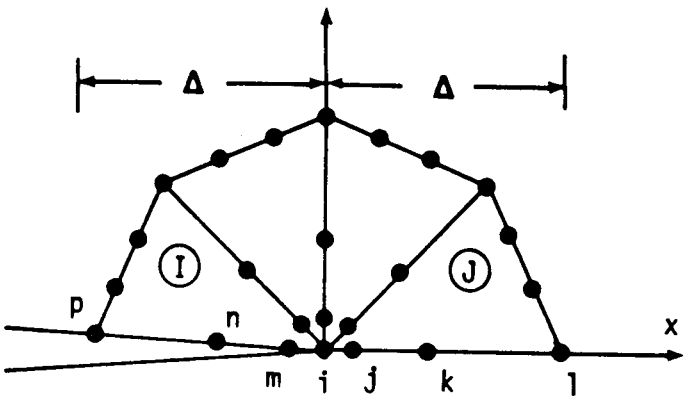

(d) Collapsed cubic singularity element

Fig. 4 - Singularity elements

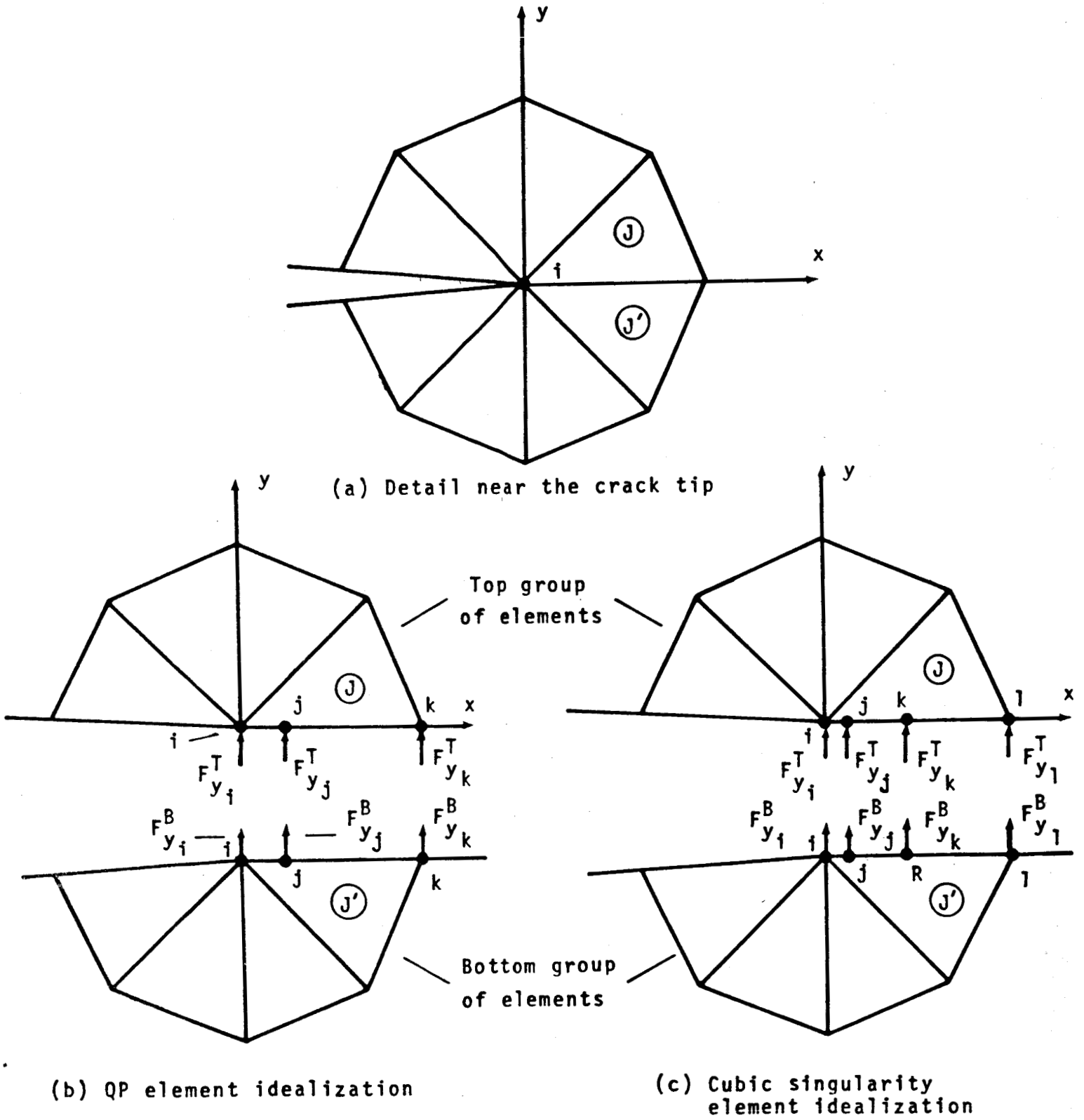

Fig. 5 - Forces at and ahead of the crack tip

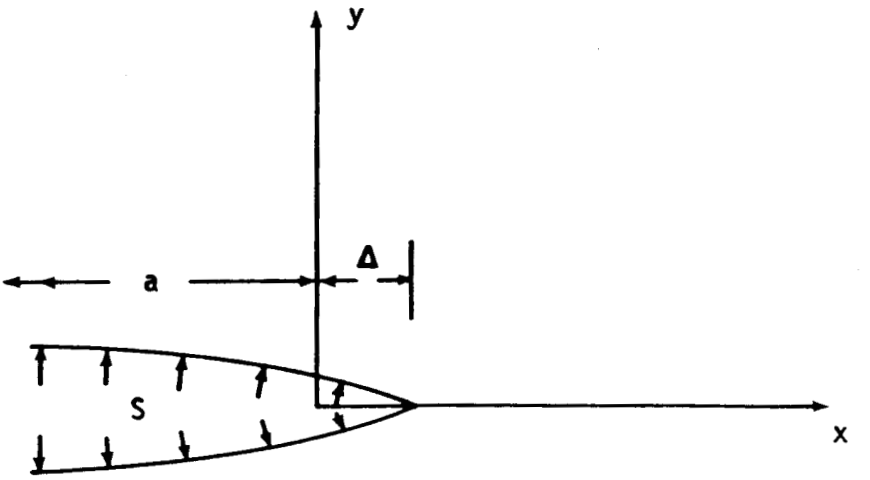

(a) Crack face pressure loading

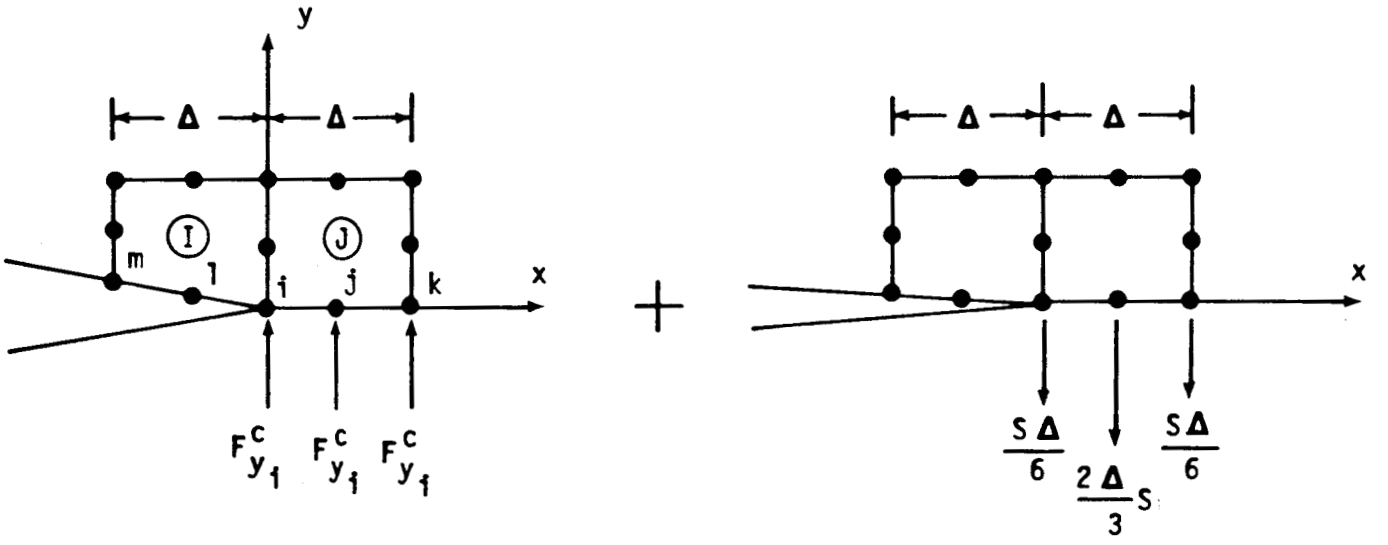

(b) Superposition of computed forces and forces needed to erase the pressure loading

Fig. 6 - Modification of forces for uniform crack face pressure loading

Non-singular elements

Singularity elements

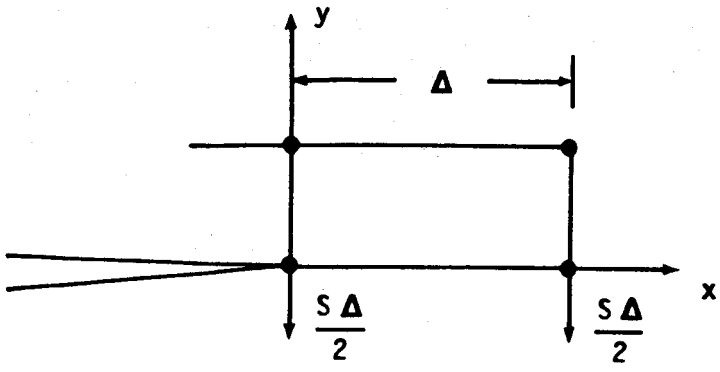

4-noded quadrilateral element

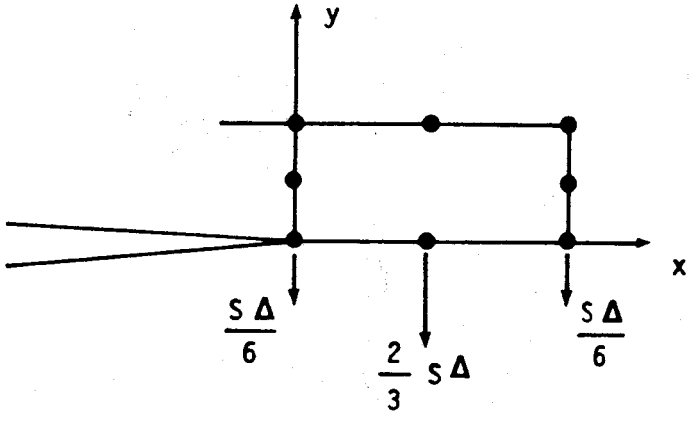

8-noded parabolic element

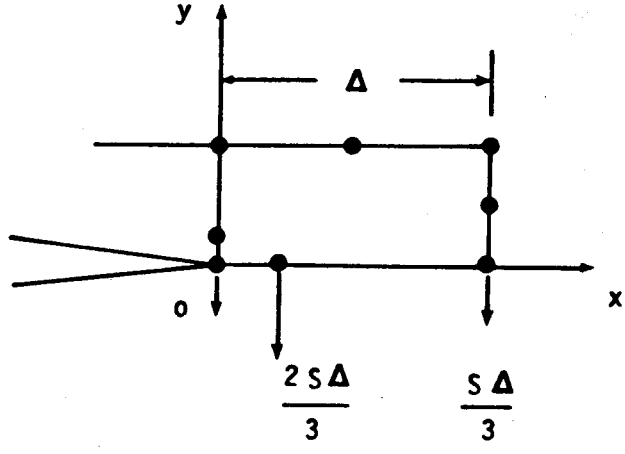

QP singularity element

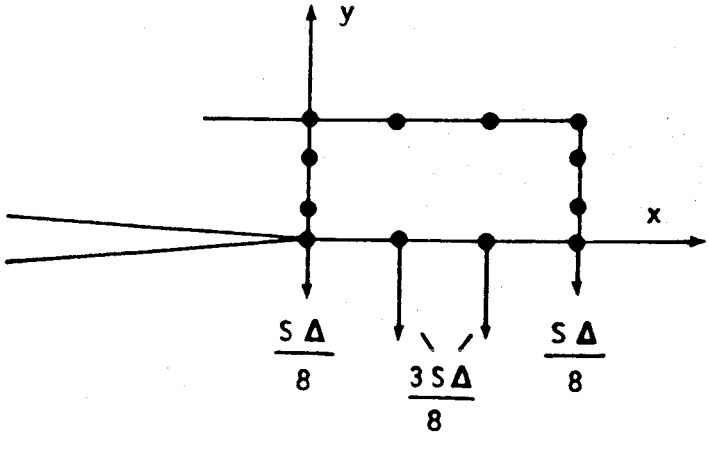

12-noded cubic element

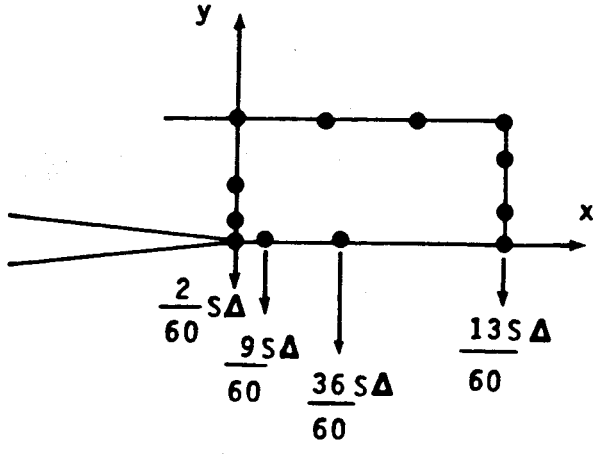

Cubic singular element

Fig. 7 - Consistent nodal forces for uniform pressure loading in various elements

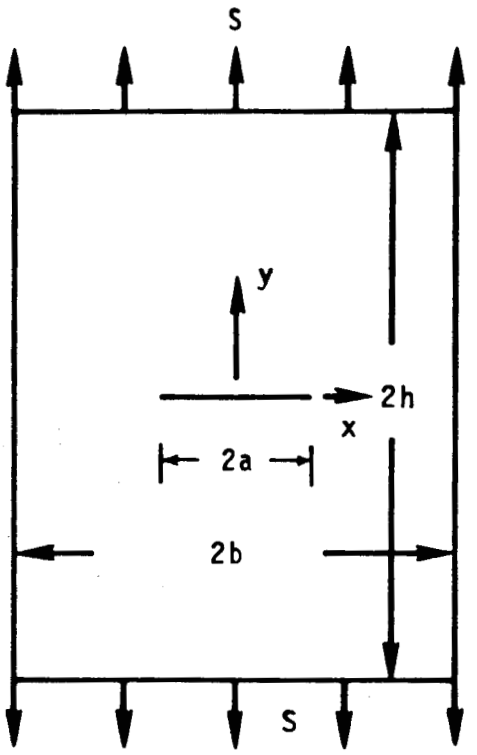

(a) CCT specimen
(h/b = 2.0; a/b = 0.8)

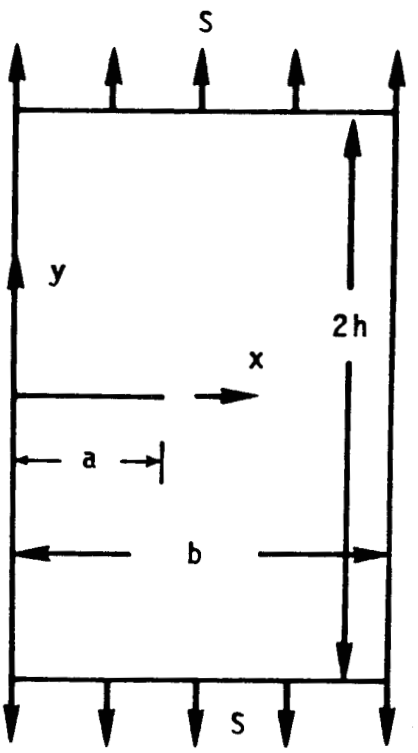

(b) SEN specimen
(h/b = 1.0; a/b = 0.8)

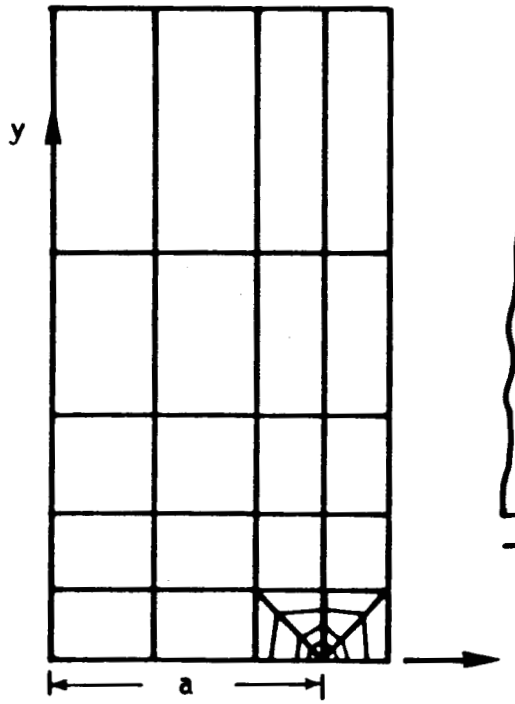

(c) Finite element model
(34 elements)

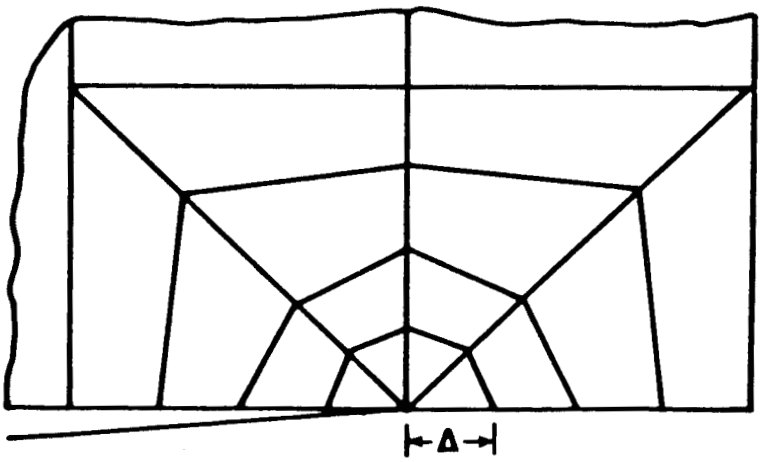

(d) Detail near the crack tip
(Δ/a = 1/16)

Fig. 8 - Mode I problems and the finite element idealization

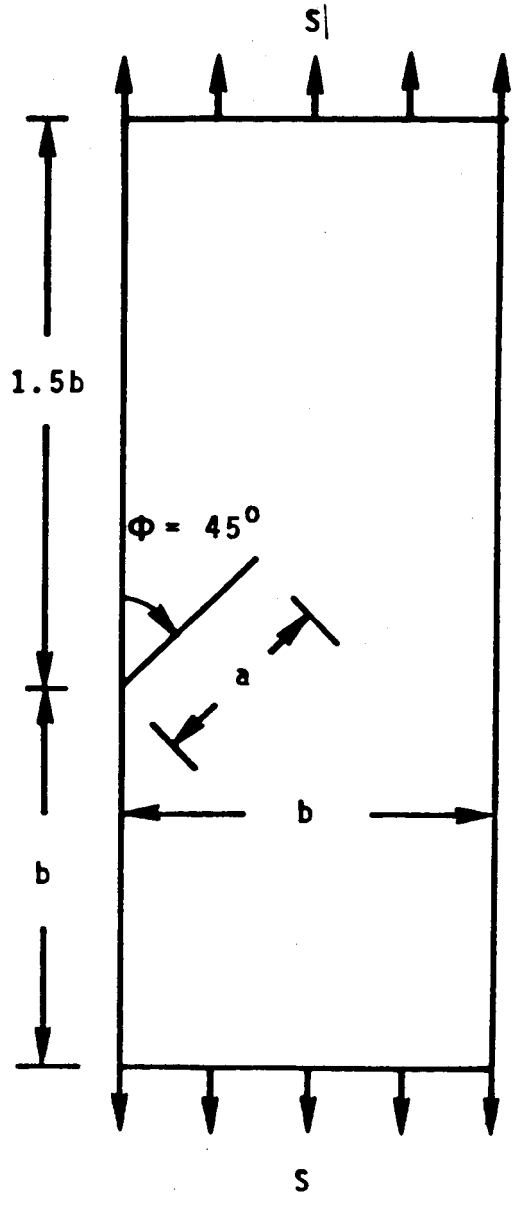

(a) Angle crack in a finite plate
(a/b = 0.5)

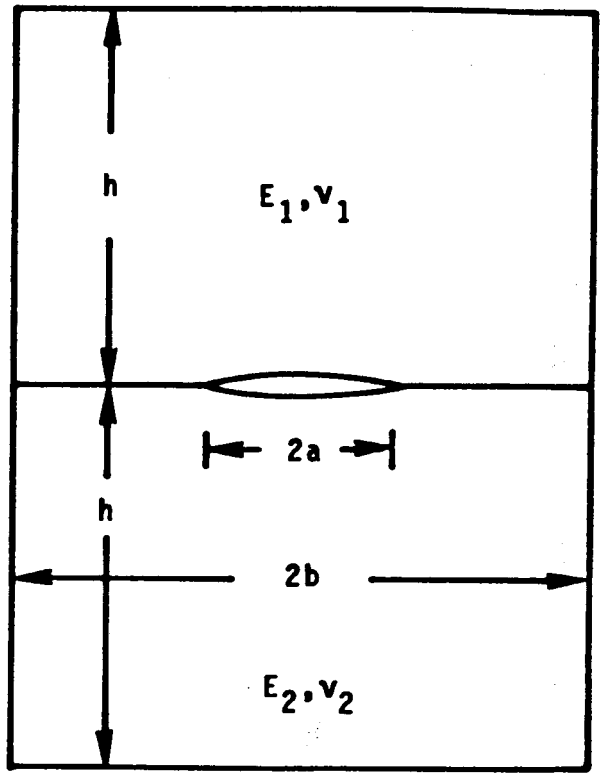

(b) Bimaterial plate with a central crack
(h/b = 1.5; a/b = 0.1; uniform crack face pressure loading, S)

Fig. 9 - Mixed mode problems

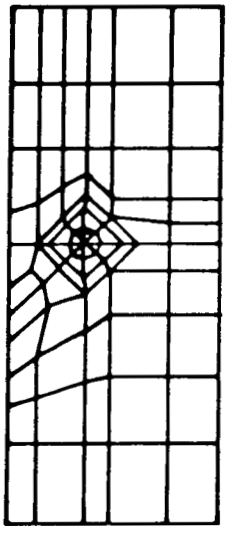

(a) Model with 8-noded parabolic elements (77 elements)

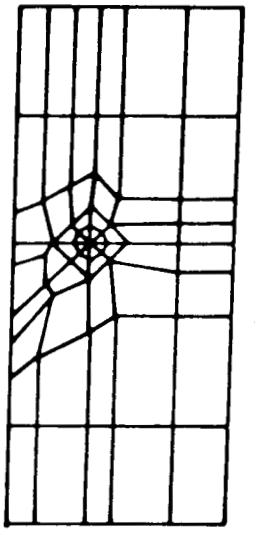

(b) Model with 12-noded cubic elements (66 elements)

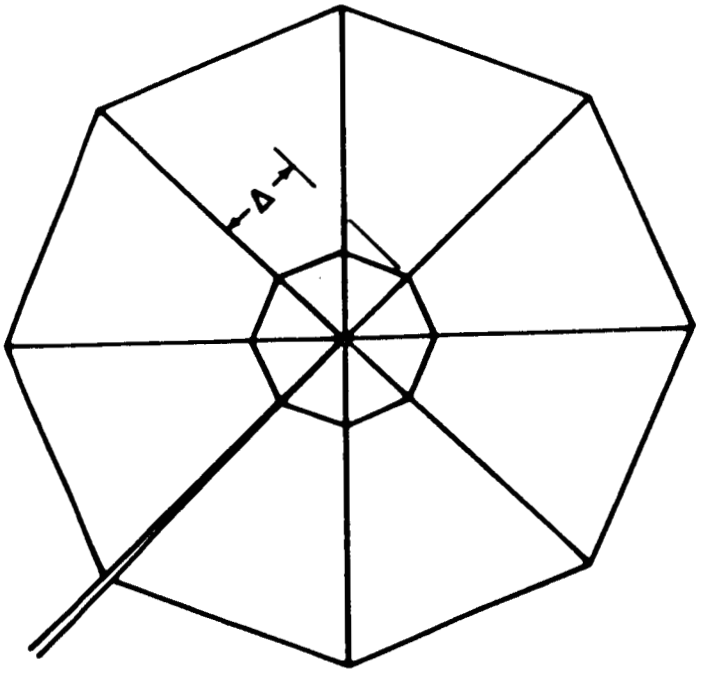

(c) Details of modeling near the crack tip

Fig. 10: Finite Element Models for the Angle Crack Problem

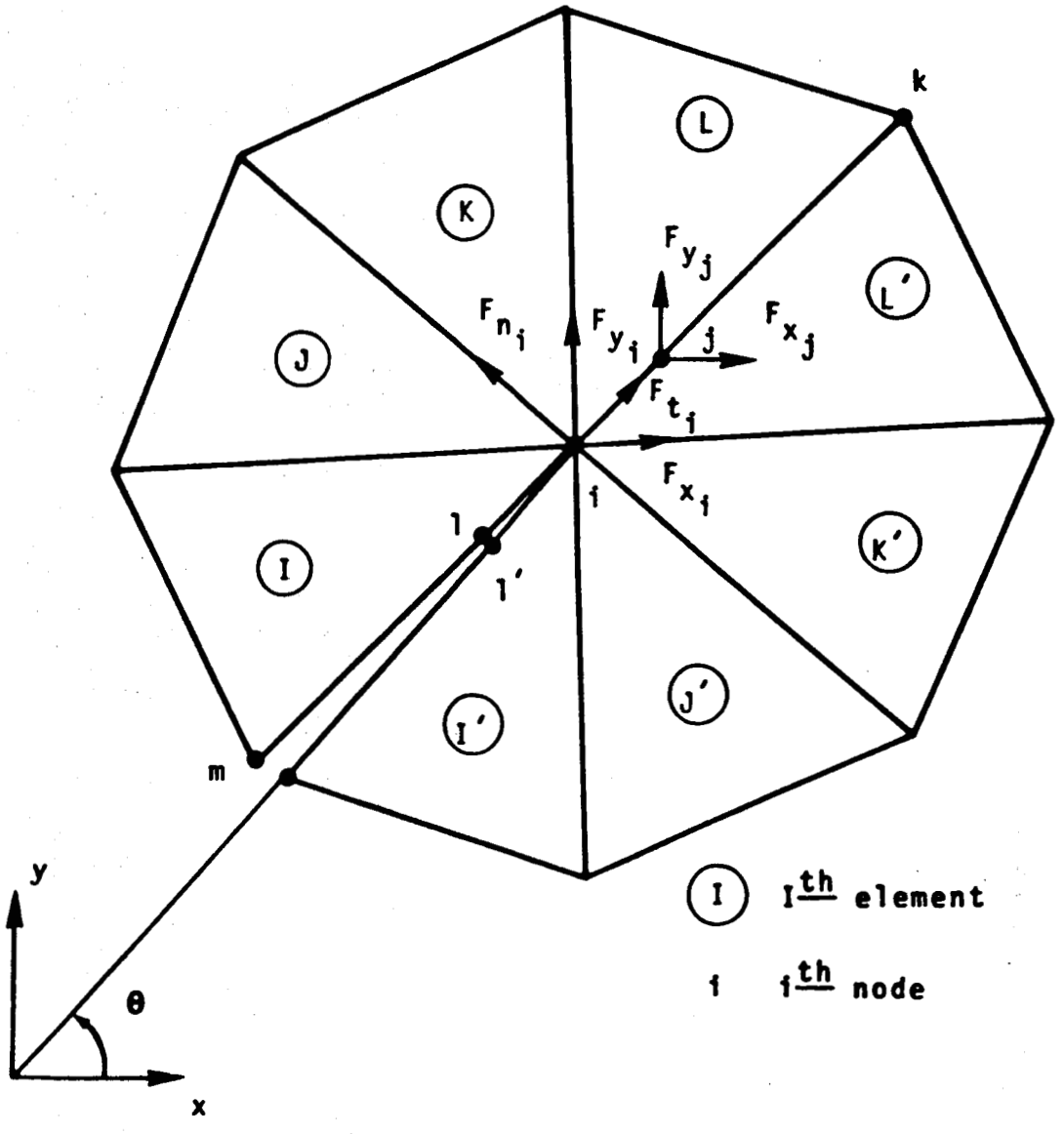

Fig. 11: Computation of Normal and Tangential Forces

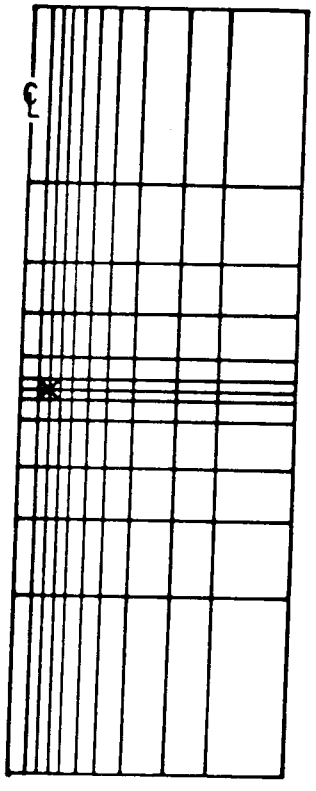

(a) Finite element model
(140 elements)

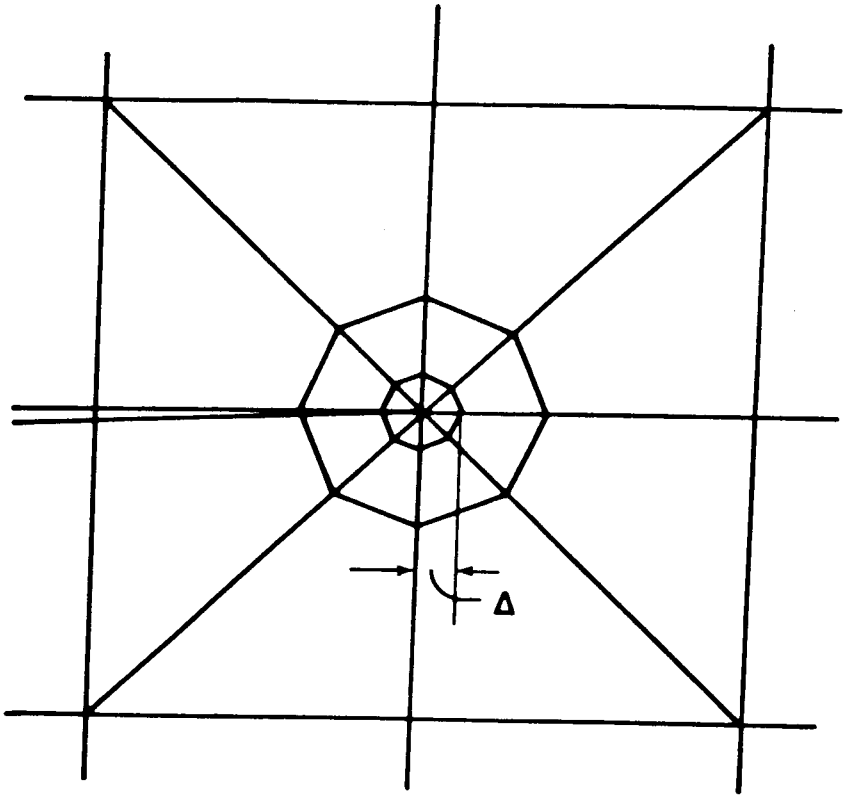

(b) Detail of modeling near
the crack tip
$\Delta/a = 0.05$

Fig. 12: Finite Element Idealization for the Bimaterial Plate Problem

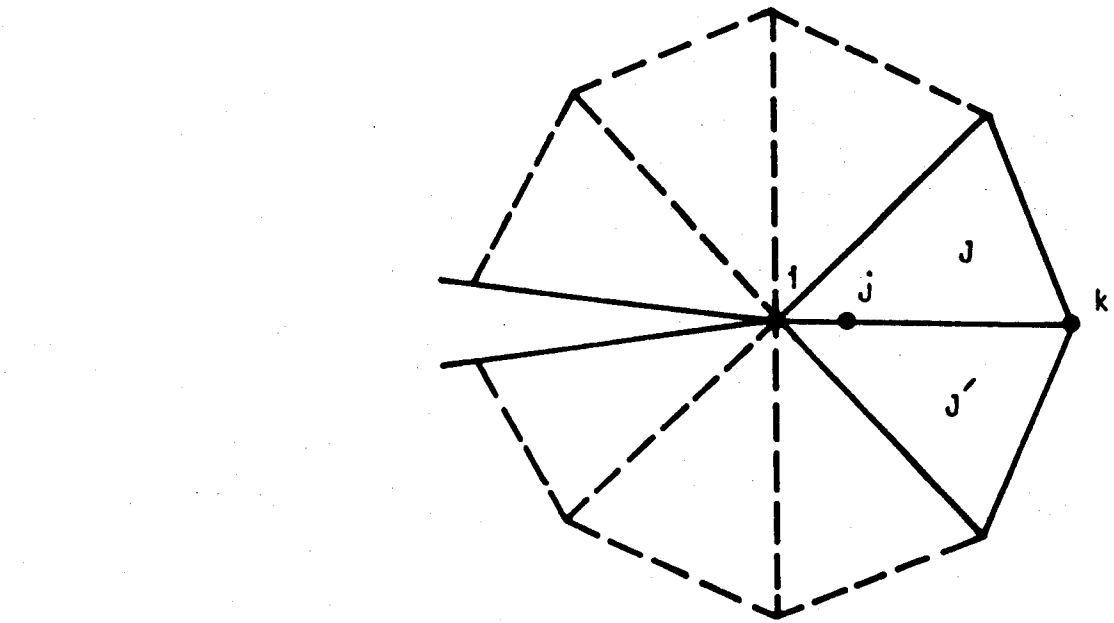

(a) Modeling at the crack tip

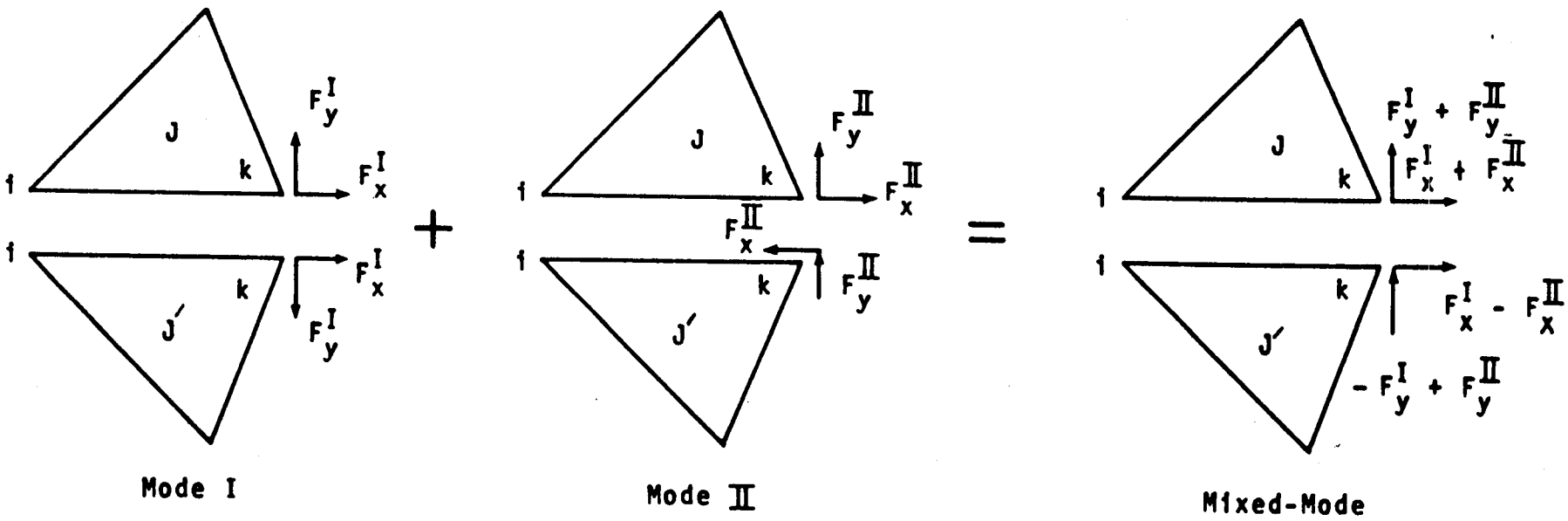

(b) Superposition of forces

Fig. 13 - Superposition to obtain forces at node k in mixed mode conditions

1. Report No.	2. Government Accession No.	3. Recipient's Catalog No.
NASA CR-178186		

4. Title and Subtitle	5. Report Date
Simple Formulas for Strain-Energy Release Rates with Higher Order and Singular Finite Elements	December 1986
	6. Performing Organization Code

7. Author(s)	8. Performing Organization Report No.
I. S. Raju	
	10. Work Unit No.

9. Performing Organization Name and Address	11. Contract or Grant No.
Analytical Services & Materials, Inc. 28 Research Drive Hampton, VA 23666	NAS1-17808 and NAS1-18256
	13. Type of Report and Period Covered
12. Sponsoring Agency Name and Address National Aeronautics and Space Administration Washington, DC 20546	Contractor Report
	14. Sponsoring Agency Code 505-63-01-05

15. Supplementary Notes

Langley Technical Monitor: C. A. Bigelow - NAS1-17808

16. Abstract

A general finite element procedure for obtaining strain-energy release rates for crack growth in isotropic materials is presented. The procedure is applicable to two-dimensional finite element analyses and uses the virtual crack-closure method. The procedure was applied to non-singular 4-noded (linear), 8-noded (parabolic), and 12-noded (cubic) elements and to quarter-point and cubic singularity elements. Simple formulas for strain-energy release rates were obtained with this procedure for both non-singular and singularity elements. The formulas were evaluated by applying them to two mode I and two mixed mode problems. Comparisons with results from the literature for these problems showed that the formulas give accurate strain-energy release rates.

17. Key Words (Suggested by Author(s))	18. Distribution Statement
Finite element analysis Two-dimensional analysis Strain-energy release rates Stress-intensity factors Non-singular elements	Unclassified - Unlimited Subject Category 39

19. Security Classif. (of this report)	20. Security Classif. (of this page)	21. No. of Pages	22. Price*
Unclassified	Unclassified	60	A04

*For sale by the National Technical Information Service, Springfield, Virginia 22151